Materials Chemistry and Physics 345 (2025) 131225

Contents lists available at ScienceDirect

Materials Chemistry and Physics

journal homepage: www.elsevier.com/locate/matchemphys

# Novel synthesis of MIL-101(Cr) with magnetized water for enhanced performance and adsorptive elimination of ibuprofen: Optimization by central composite design

Sara Abolhasani [a,b], Ali Ahmadpour [a,b,*], Mostafa Gholizadeh [c]

[a] Department of Chemical Engineering, Faculty of Engineering, Ferdowsi University of Mashhad, Mashhad, 91779-48944, Iran
[b] Industrial Catalysts, Adsorbents, and Environment Lab., Oil and Gas Research Institute, Ferdowsi University of Mashhad, Mashhad, Iran
[c] Department of Chemistry, Faculty of Science, Ferdowsi University of Mashhad, Mashhad, 91779-48974, Iran

## HIGHLIGHTS

- Magnetized water was used for MIL-101 (Cr) synthesis using the hydrothermal method.
- Optimized magnetic field exposure time applied to water by influencing the properties of MIL-101(Cr).
- The synthesized adsorbent effectively removed ibuprofen from aqueous solutions.
- Adsorption kinetics followed the pseudo-second-order and Langmuir isotherm models.

## GRAPHICAL ABSTRACT

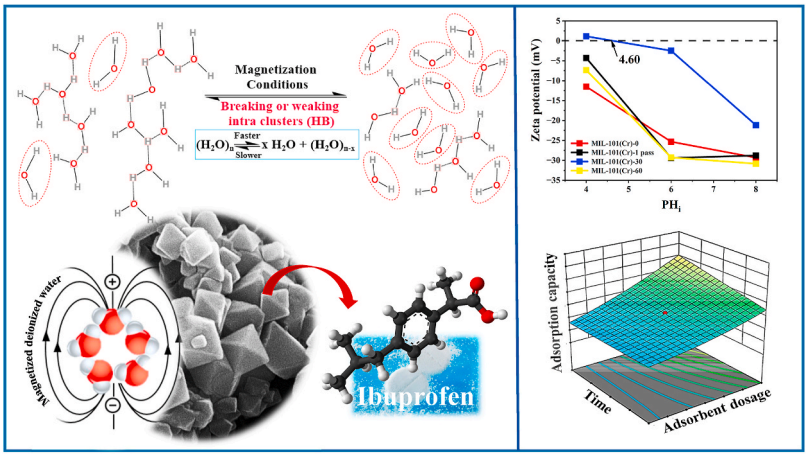


## ARTICLE INFO

*Keywords:*
Magnetized water
MIL-101(Cr)
Ibuprofen
Adsorption
Central composite design

## ABSTRACT

In this study, a magnetic field was applied to deionized water to produce magnetized deionized water, which was utilized for the first time in the hydrothermal synthesis of MIL-101(Cr). The magnetized deionized water acted as a synergistic solvent, leading to the formation of a highly porous and stable metal-organic framework (MOF). Different magnetization durations were applied to the deionized water to achieve the optimal crystal structure with enhanced performance. The prepared MOF, with an appropriate surface area and meso/microporous structure, was used to adsorb ibuprofen (IBP) from an aqueous solution. Techniques including FTIR, XRD, FESEM, BET, and zeta potential were used for characterizing the adsorbent. The prepared MIL exhibited a surface area of 3257 $m^2 g^{-1}$ and a smooth octahedral molecular geometry when synthesized using 30 min of magnetizing deionized water. The adsorption capacity of ibuprofen by the parent MIL-101(Cr) increased from 76.67 to 92.47 mg $g^{-1}$ under optimal conditions (pH = 4.5, contact time = 30 min, and adsorbent dose = 0.125 g $L^{-1}$), when

* Corresponding author. Department of Chemical Engineering, Faculty of Engineering, Ferdowsi University of Mashhad, Mashhad, 91779-48944, Iran.
*E-mail address:* Ahmadpour@um.ac.ir (A. Ahmadpour).

https://doi.org/10.1016/j.matchemphys.2025.131225
Received 18 March 2025; Received in revised form 13 June 2025; Accepted 1 July 2025
Available online 6 July 2025

compared to MIL-101(Cr)-30. Under these conditions, the MIL-101(Cr) treated with 30 min magnetized water demonstrated up to a 15 % higher removal efficiency than the unmodified MIL-101(Cr), which can be attributed to its enhanced surface area and the shift in the $pH_{pzc}$ point resulting from the use of magnetized water during synthesis. The optimization of variables affecting the removal process was investigated using the central composite response surface method (RSM-CCD). In addition, pseudo-second-order (Ho) kinetic and Langmuir isotherm models were established with the spontaneous mechanism ($\Delta G < 0$) of IBP on MIL-101(Cr)-30. Finally, the reusability of the adsorbent is five times due to the low amount of adsorbent (0.125 g $L^{-1}$), which indicates the excellent potential of the modified adsorbent in eliminating IBP from aquatic environments.

## 1. Introduction

Water pollution and environmental issues are among global concerns, as they pose serious threats to human, animal, and plant health [1]. Industrialization and urbanization have led to increased discharge of waste and pollutants into surface and groundwater resources [2,3]. Among various pollutants, pharmaceuticals are considered a significant contributor to the contamination of aquatic environments [4].

Ibuprofen (IBP) is a class of nonsteroidal anti-inflammatory drugs (NSAID) used to diminish fever, relieve pain, and improve inflammation. High amounts of ibuprofen in drinking water can cause digestive, liver, and kidney problems in humans due to bioaccumulation [1,2]. Also, these compounds are toxic to aquatic animals [4]. Because of these hazards and the low solubility of approximately 21 mg $L^{-1}$ at 25 °C, effective water treatment methods must be used [5]. Adsorption method with the efficiency of reusability, low cost, and high scale has been considered in many research studies for purifying water by removing pollutants [6–8].

Metal-organic frameworks (MOFs) are classified as crystalline and porous adsorbents composed of metal clusters grafting to organic linkers [9]. The geometric properties of these adsorbents, including adjustable surface area, pore volume, and low density, demonstrate their efficiency in removing contaminants from aqueous solution [10–12].

MIL-101(Cr), one of the types of metal-organic framework (MOF) based on chromium terephthalate, composed of chromium metal ions and a terephthalic acid linker, was first studied by Ferey et al., in 2005 [13]. Recently, these innovative porous materials have attracted interest in water treatment due to their tunable pore structure, water stability, and high uptake capacity [14–16]. Hydrothermal and solvothermal synthesis are the most common methods of preparing these adsorbents using different solvents like hydrofluoric acid (HF), hydrochloric acid (HCl), nitric acid ($HNO_3$), acetic acid, etc. [17]. Hu et al. introduced porous MIL-101(Cr) using hydrochloric acid (HCl) instead of hydrofluoric acid (HF) as the mineralizer in the synthesis process due to the toxic properties of HF [18]. Zhao et al. reported that MIL-101(Cr) with a suitable surface area and nano-sized structure utilized acetic acid as a mineral agent [19]. The solvent is a key parameter in the synthesis of porous materials, as it influences both the metal ions and the linker in the solution. Changes in solvent properties, such as viscosity and surface tension, can affect the nucleation rate and crystal size [20–22]. To date, numerous studies have been conducted on the removal of the pollutant ibuprofen using metal-organic frameworks and their composites. Zhuo et al. employed two types of composite beads, MIL-101(Cr)/sodium alginate and MIL-101(Cr)/chitosan, to remove ibuprofen from aqueous solutions. Their adsorption capacities were around 70 mg $g^{-1}$ and 35 mg $g^{-1}$, respectively [23]. Seo et al. conducted a brief study on the adsorption of ibuprofen from aqueous media using MIL-101 and its functionalized forms, MIL-101-OH and MIL-101-$NH_2$. The results indicated that the adsorption capacity ranged from 30 to 50 mg $g^{-1}$ after 12 h for these MOFs [24]. In their study, Sun et al. reported adsorption capacities of 127.1 mg $g^{-1}$ and 50.69 mg $g^{-1}$ for the elimination of ibuprofen using UiO-66 and UiO-66-$NH_2$ metal-organic frameworks, respectively, under equilibrium conditions after 10 h [25]. Alkhatami et al. demonstrated that zirconium metal-organic frameworks (Zr-MOFs) and their functional modification (Zr-MOF-$NH_2$) exhibit great potential for removing IBP from wastewater, with adsorption capacities of 384.69 mg $g^{-1}$ and 371.34 mg $g^{-1}$, respectively, under endothermic and spontaneous conditions after 100 min [4].

Magnetized deionized water (MDW) is produced when deionized water is passed through a solvent magnetizing apparatus (SMA) [26]. Adjusting the magnetization time and magnetic field intensity can improve the physicochemical properties of water [27,28]. Reduction of surface tension and increase of density of water can occur using magnetic treatment [29,30]. In addition, the magnetic field affects the pH, zeta potential, and hydrogen bonding, causing increases in the dispersion of particles in the solution [31,32]. In the last few years, magnetized deionized water has been used in various fields such as livestock and poultry [33,34], agriculture [35–38], concrete [39,40], oil recovery [41], chemistry [20,42–44], and so on due to its greenness, cost-effective, and simple operating process.

This work synthesized MIL-101(Cr) with magnetized deionized water as a solvent using the hydrothermal method. Different magnetization times were induced on deionized water, and its effect on adsorbent morphology was investigated. The primary goal of this research is to propose magnetized deionized water (MDW) as a condition to improve synthesis, thereby reducing the reliance on expensive chemicals used in the production of composite nanostructures. Despite the substantial body of research on the removal of pharmaceutical pollutants from aqueous solutions, comprehensive studies focusing on both isotherm and kinetic and thermodynamic studies for the removal of ibuprofen using raw MIL-101(Cr) remain sparse. This study aims to bridge this gap by selecting ibuprofen as the model pharmaceutical pollutant. Additionally, we employ the response surface method (RSM) to optimize the operating conditions, achieving the most efficient removal process.

## 2. Materials and methods

### 2.1. Preparation of magnetized deionized water

The properties of deionized water were improved by passing it through a solvent magnetizing apparatus (SMA) in the presence of a 0.65 T (6500 Gauss) magnetic field. This instrument has two solvent

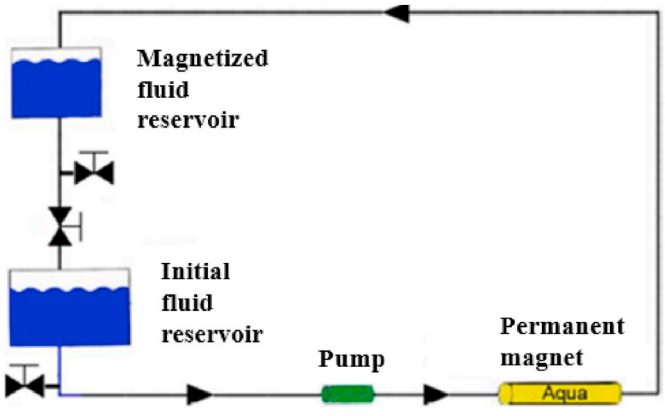


**Scheme 1.** Schematic of solvent magnetizing apparatus (SMA) [20].

reservoirs connected to each other with a valve. As shown in Scheme 1, the solvent can flow in a closed cycle by a centrifugal pump and pass directly across a magnetic field (AQUA CORRECT, H.P.S Co., Germany). Following the closure of the valve separating the reservoirs, 2.5 L of deionized water was poured into the lower reservoir. The pump is then activated, and the solvent flows through the magnetic field at a rate of 500 mL $s^{-1}$, collecting in the upper reservoir within 5 s. This is referred to as deionized water that has undergone a single pass through the magnetic field. In the next steps, to increase the duration of exposure to the magnetic field, deionized water is magnetized by circulating it through the field multiple times at 30 and 60 min intervals. These solvents are then used for hydrothermal synthesis. Lastly, the surface characteristics and adsorption capacity of the MIL-101(Cr) adsorbent are examined at each time point. The complete description of the device is given in a U.S. patent (US10507450B2) [45]. Magnetized deionized water in a controlled closed cycle is named as follows:

1. Ordinary water (MW-0)
2. One pass magnetized water (MW-1 pass)
3. Magnetized water for 30 min (MW-30)
4. Magnetized water for 60 min (MW-60)

### 2.2. Materials

Chromium (III) nitrate nonahydrate ($Cr(NO_3)_3.9H_2O$, 97 %), 1,4-benzenedicarboxylic acid ($H_2BDC$, 99 %), and acetic acid ($C_2H_4O_2$, >97 %) were all sourced from Sigma-Aldrich. Ammonium fluoride ($NH_4F$) and N–N, dimethylformamide (DMF, 99 %) were purchased by Merck, and ethanol (EtOH, 96 %) by Drm-Chem (Iran). Also, deionized (DI) water of the highest purity for magnetization and ibuprofen ($C_{13}H_{18}O_2$, Sigma-Aldrich) were used for the experiments.

### 2.3. Preparation of MIL-101(Cr)

The main procedure for MIL-101(Cr) synthesis was adopted with some modifications according to the method presented by Yu et al. [46]. Briefly, 3.46 g chromium (III) nitrate nonahydrate, 1.4 g terephthalic acid, and 0.5 $cm^3$ acetic acid were mixed in 43 $cm^3$ ordinary and magnetized water, respectively. As mentioned, magnetized deionized water was used at different times, such as 1 pass, 30 min, and 60 min. Acetic acid was used as a mineral agent. After sonication for 1 h, the mixture was heated at 220 °C for 8 h in a 65 $cm^3$ stainless-steel autoclave. Finally, the green precipitate was separated by centrifugation of the solution.

Impurities and unreacted components were removed as follows: twice washing with 80 $cm^3$ water, DMF, and ethanol, respectively, was adopted, and then once with 40 $cm^3$ $NH_4F$. Finally, the product was recovered by centrifuge and heated at 70 °C for 15 h overnight. samples were named MIL-101(Cr)-X, where X corresponds to the magnetization duration of solvent in the synthesis (X: 0, 1 pass, 30, and 60). The preparation step of the synthesized adsorbent is depicted in Scheme 2.

### 2.4. Characterization

The crystal pattern was studied by X-ray Diffraction spectroscopy (XRD, D8-Advance Bruker Cu Kα1 λ = 0.15406 nm). The mean crystallite size of the prepared samples was calculated using the Debye-Scherrer equation (Eq. (1)) [47]:

$$D = \frac{K\lambda}{\beta \cos\theta} \quad (1)$$

where D represents the crystallite size, K is the Scherrer constant (K = 0.94), λ is the wavelength of the X-ray used (λ = 0.0.15406 nm), β denotes the full width at half maximum (FWHM) of the diffraction peak, and θ is the Bragg angle. Fourier-transform infrared spectroscopy (FTIR, Thermo Nicolet Avatar 360, USA) was utilized to determine the chemical bond of the adsorbent in the range of 400–4000 $cm^{-1}$. The morphology of samples was analyzed by a Field Emission Scanning Electron Microscope (FESEM, Tescan Mira3 FEG). Also, the elements are detected with an EDS/EDX analysis. The surface area and pore volume of MIL-101(Cr) were measured by data obtained from the nitrogen adsorption-desorption technique using the Brunauer-Emmett-Teller method (BELSORP MINI II), and the distribution of pore size was evaluated by the Barrett-Joyner-Halenda (BJH) method. Zeta potential (Zetacompact, CAD) was used to measure the surface charge of the prepared MOFs. pH adjustment in the experiments was done with a HANNA pH meter. Ionic conductivity was measured using a Metrohm 712 conductometer (Switzerland). Viscosity measurements were performed using an Ubbelohde viscometer with a calibration constant of 0.00446 ($mm^2 s^{-2}$). The contact angle of ordinary and magnetized water was measured on a chemically inert and hydrophobic graphite surface, which was selected as the reference surface to evaluate subtle changes in wettability. Measurements were averaged from at least three trials using 4 μL droplets at three distinct locations on the surface. All physicochemical properties were measured at 20 ± 5 °C.

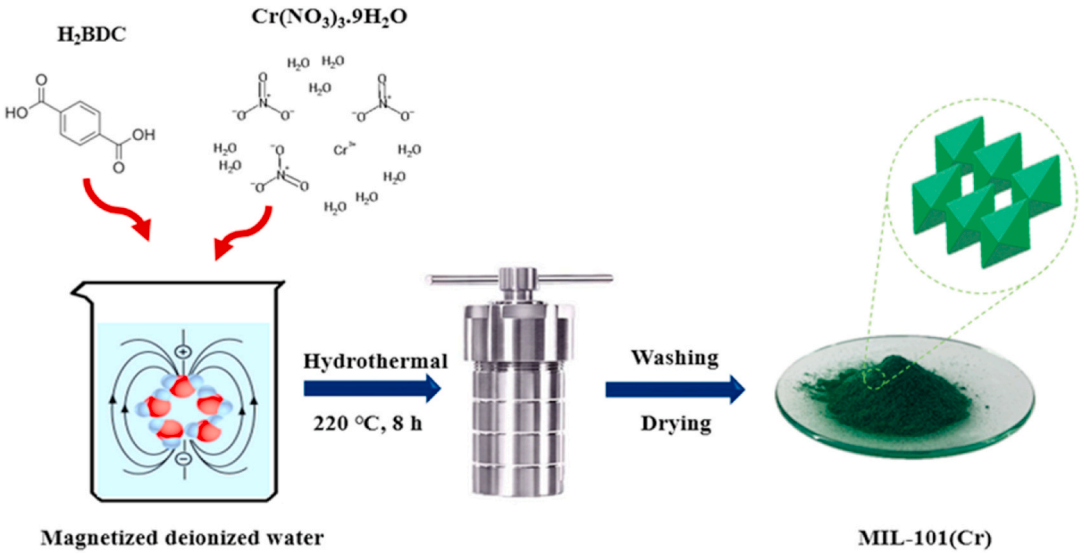


**Scheme 2.** Preparation step of MIL-101(Cr) as prepared.

### 2.5. Determination of the zero charge point

The isoelectric point or $pH_{pzc}$ of the adsorbent was determined at three pH points (4, 6, and 8) to assess the surface charge. The pH adjustment was accomplished using aqueous HCl and NaOH solutions at 1 M and 0.1 M, respectively. The point of zero charge ($pH_{pzc}$) was identified as the pH value where the final pH ($pH_{final}$) equals the initial pH ($pH_{initial}$), resulting in a zero difference [8].

### 2.6. Adsorption experiments

Batch systems of ibuprofen solution at 10 mg $L^{-1}$ concentration were performed. Synthesized MIL-101(Cr) was added to 40 $cm^3$ IBP solution for adsorption experiments. After adsorption, an Analytic Jena-Spekol 1300.1 UV–Vis spectrophotometer operating at a peak of 224 nm was used to determine the remaining sample. A calibration curve was utilized to extract the data. The following equations (Eqs. (2) and (3)) were used to determine the yield of removal (R%) and equilibrium adsorption capability $q_e$ (mg $g^{-1}$) [5]:

$$R\% = \frac{(C_0 - C_e)}{C_0} \times 100 \tag{2}$$

$$q_e = \frac{(C_0 - C_e)V}{W} \tag{3}$$

where $C_0$ denotes the initial concentration and $C_e$ (mg $L^{-1}$) is the equilibrium concentration of ibuprofen. Also, V (L) and W(g) are the volume and adsorbent dose, respectively.

### 2.7. Design of experiment

The effects of various parameters, including pH, contact time, and adsorbent dose, on the removal of IBP need to be examined. All these independent parameters were coded by Design-Expert 12 software, and the experiments were optimized by central composite design (CCD). Table 1 shows the level of variables from high (+1) to low (1). It should be noted that the desired value of alpha (α) equal to 1.5 was selected in the range of pH (4–8), contact time (10–30 min), and adsorbent dose (0.025–0.25 g $L^{-1}$) to study the removal of IBP.

The reaction response between independent parameters was analyzed using analysis of variance (ANOVA). The second-order polynomial equation (Eq. (4)) fitted the data following the model [5].

$$Y = \beta_0 + \sum_{i=1}^{k} \beta_i x_i + \sum_{i=1}^{k} \beta_{ii} x_{ii}^2 + \sum_{i=1}^{k} \sum_{i \neq j=1}^{k} \beta_{ij} x_i x_j \tag{4}$$

in the above equation, Y is the reaction outcome (adsorption capacity), parameters $x_i$ and $x_j$ are the operating parameters (pH, contact time, and adsorbent dose). $\beta_0$ is the cutoff point in the regression model. In addition, $\beta$i, $\beta$ii, and $\beta$ij represent linear, second-order, and interaction coefficients [48,49].

**Table 1**
The column information of the code and the level of variables in the CCD design.

| Name | Codes | levels | | | | |
|---|---|---|---|---|---|---|
| | | -α | −1 | 0 | +1 | +α |
| pH | A | 3 | 4 | 6 | 8 | 9 |
| Contact time (min) | B | 5 | 10 | 20 | 30 | 35 |
| Adsorbent dose (g $L^{-1}$) | C | 0.025 | 0.0625 | 0.1375 | 0.2125 | 0.25 |

## 3. Results and discussion

### 3.1. Effect of magnetized deionized water on MIL-10(Cr) preparation

Different magnetization durations of deionized water were applied in the synthesis of MIL-101(Cr) to evaluate the IBP removal efficiency and compare it with that of the parent MIL-101(Cr). Water samples labeled MW-0, MW-1 pass, MW-30, and MW-60 were used to prepare adsorbents named MIL-101(Cr)-X, where X denotes the magnetization time of deionized water (X: 0, 1 pass, 30, and 60) used during synthesis. Therefore, similar conditions, including pH = 7, contact time = 30 min, and different adsorbent doses, were used in 40 $cm^3$ IBP (10 mg $L^{-1}$) to remove contaminants from the aqueous solution. The details of these pre-tests are reported in Table 2. Among these synthesized samples, MIL-101(Cr)-30 with desirable removal efficiency and optimal magnetization time was selected for the experiment design. Therefore, characterization and statistical analysis were performed for these samples, which are detailed in the following sections.

### 3.2. Physicochemical properties of magnetized deionized water

The physicochemical properties of ordinary and magnetized water are summarized in Table 3. Based on laboratory measurements and observations, minor yet measurable changes were detected in these properties following magnetic treatment. These variations are likely attributed to modifications in the cluster structure of water molecules resulting from alterations in the hydrogen bonding network as well as a temporary shift in the ionic equilibrium between $H^+$ and $OH^-$ ions [50,51]. Given that deionized water was used, which does not contain any significant dissolved ions, it is reasonable to assume that the observed changes primarily affect the physical and intermolecular characteristics of water rather than its chemical composition. However, these changes are generally subtle and transient, as water molecules tend to return to their equilibrium state over time. Accordingly, it is expected that the magnitude of these effects will decrease or reach a steady state as the magnetization time increases, a phenomenon commonly known as the "magnetic saturation effect" [52].

The observed reduction in dynamic viscosity observed under magnetic treatment is attributed to the disruption of hydrogen-bonded water clusters by the applied magnetic field. This structural rearrangement enhances molecular mobility, decreases internal resistance to flow, and consequently leads to a gradual and relatively uniform decline in viscosity [53]. Furthermore, the slight decrease in contact angle indicates that magnetic treatment facilitates molecular and surface changes, increases water polarity, and reduces surface tension.

### 3.3. Characterization of adsorbents

The XRD pattern of MIL-101(Cr)-0, MIL-101(Cr)-30, and simulated-MIL-101(Cr) are shown in Fig. 1. As can be seen, the diffraction peaks for the samples occurred at 2θ of 3.2, 5.2, 6, 9.1, and 16.6. These patterns match well with the modeled MIL-101(Cr) pattern described in the literature [54,55]. Therefore, the synthesis has occurred correctly. No distinct peak after 2θ of 17 was identified for MIL-101(Cr)-30, which belongs to terephthalic acid. MIL-101(Cr)-30 has narrow and sharp

**Table 2**
Comparison of adsorbent efficiency on different doses.

| Dose (g $L^{-1}$) | Removal efficiency (R%) | | | |
|---|---|---|---|---|
| | MIL-101 (Cr)-0 | MIL-101(Cr)-1pass | MIL-101(Cr)-30 | MIL-101(Cr)-60 |
| 0.0625 | 46 | 56 | 58 | 66 |
| 0.125 | 66 | 76 | 88 | 100 |
| 0.1875 | 89 | 88 | 98 | 100 |
| 0.25 | 100 | 100 | 100 | 100 |

**Table 3**
Physicochemical properties of ordinary and magnetized deionized water.

| Properties of deionized water | Ordinary | Magnetized | | |
|---|---|---|---|---|
| | | 1 pass | 30 min | 60 min |
| Ionic conductivity (μS $cm^{-1}$) @ 20 °C | 1.399 ± 0.02 | 1.885 ± 0.02 | 1.639 ± 0.02 | 1.520 ± 0.02 |
| Density (g $cm^{-3}$) | 0.9981 ± 0.003 | 1.0086 ± 0.003 | 1.0045 ± 0.003 | 0.9781 ± 0.003 |
| pH @ 20 °C | 5.85 | 6.37 | 6.55 | 6.90 |
| Viscosity (mPa $s^{-1}$) @ 20 °C | 1.0014 ± 0.003 | 0.9356 ± 0.003 | 0.9049 ± 0.003 | 0.8681 ± 0.003 |
| Contact angle between water and graphite (degrees) | 92.27 | 91.45 | 85.6 | 90.23 |

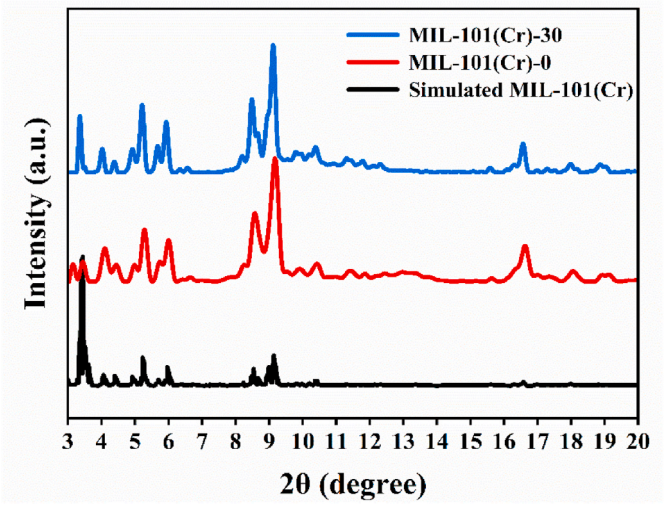


**Fig. 1.** XRD pattern of simulated-MIL-101(Cr), MI-101(Cr)-0.

peaks, which indicates that MIL-101(Cr)-30 has a more crystalline framework with a smaller particle size than MIL-101(Cr)-0 [47]. Using the Debye-Scherrer equation applied to the sharp diffraction peaks, the estimated crystallite sizes were 46.18 nm and 74.48 nm for MIL-101 (Cr)-0 and MIL-101(Cr)-30, respectively. As confirmed by BET analysis, as the crystal size increases, structural defects and agglomeration decrease, leading to better crystalline order, prevention of pore blockage, and ultimately an increase in the active surface area [56]. These results demonstrated that using magnetized deionized water leads to improved crystal growth with good integration of ions ($Cr^{3+}$) and terephthalate linkers (BDC).

The chemical groups of the synthesized adsorbents were identified by FTIR spectra, as shown in Fig. 2a. Cr–O stretching vibrations were observed at a wavenumber of approximately 580 $cm^{-1}$, which belongs to chromium ions within the structures. The observation peak at 1400 $cm^{-1}$ belongs to the O–C–O bond vibration, while the C–H stretching is acknowledged with 745 $cm^{-1}$ and 1016 $cm^{-1}$ bands. These bands illustrated the $H_2$BDC linker in the structures [6,57]. The 1508 $cm^{-1}$ band corresponds to the C═C vibration. In addition, a broad band of –OH at 3400 $cm^{-1}$ was exhibited. The intensity of this peak in treated MIL-101(Cr) was reduced due to the reduction of hydrogen bonding and accumulation of water molecules by magnetic water treatment [58]. As presented in FTIR analysis before and after IBP adsorption (Fig. 2b), there was no significant alteration in the intensity and location of the peaks. Just a slight decrease was observed in the C–O peak, which corresponds to the benzene ring. This suggests that the primary method for removing contaminants is through surface adsorption and trapping within the pores, with no evident interaction occurring between the functional groups and ibuprofen molecules.

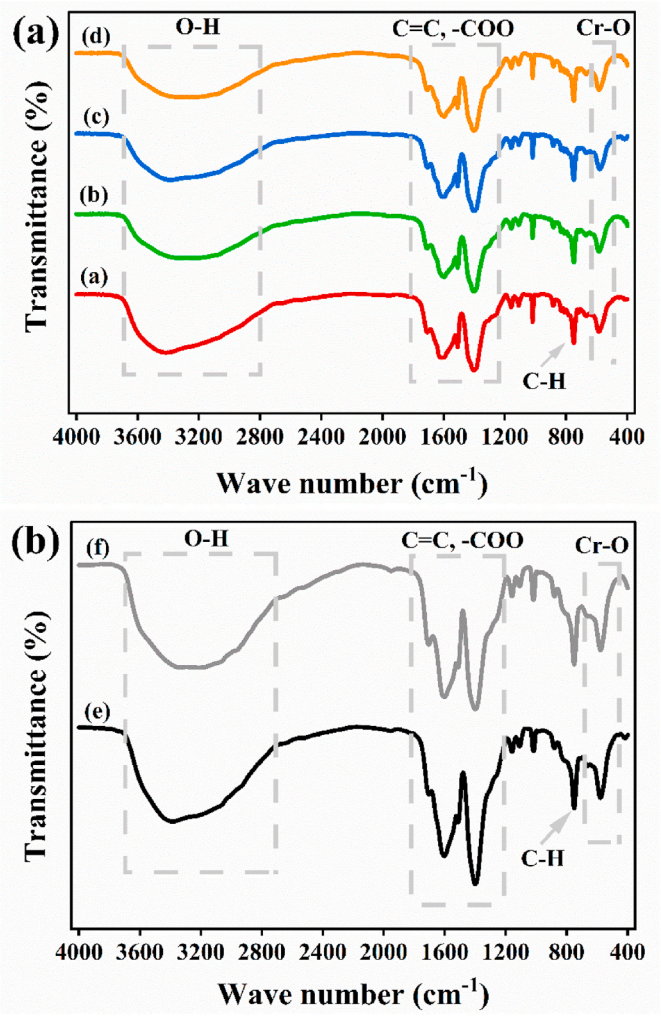


**Fig. 2.** a) FT-IR spectra of MIL-101(Cr)-X (X: 0 (a), 1 pass (b), 30 (c), and 60 (d)); b) FT-IR spectra of MIL-101(Cr)-30 before (e) and after (f) IBP adsorption.

The morphology of the mentioned MOFs was investigated using FESEM analysis (Fig. 3a–d). The smooth octahedral shape of the particles was perceived in the structure of MIL-101(Cr)-30, comparable to the literature [59]. Meanwhile, MIL-101(Cr)-0 particles showed irregular and broken morphology. A uniform crystal without any aggregates, with a particle size range of 200–300 nm, was visible in the FESEM images of MIL-101(Cr)-30. The particle size distribution was assessed by examining more than 100 particles using ImageJ software (Fig. 3e and f). The average particle size for MIL-101(Cr)-0 was 322 nm with a standard deviation of 100 nm (CV ≈ 31 %), while MIL-101(Cr)-30 showed an average size of 237 nm with a standard deviation of 50 nm (CV ≈ 21 %), indicating a narrower and more consistent size distribution in the modified sample. These results indicate that magnetization of water affects both nucleation and crystal growth mechanisms [20]. In particular, magnetized deionized water appears to enhance the nucleation rate of MOF cores and facilitate the formation of octahedral crystals. As a result, the available starting materials are distributed among more nucleation sites, which limits the growth of individual crystals and results in smaller particle sizes. In addition, the higher nucleation rate, due to more uniform growth conditions, enhances the formation of well-defined octahedral MOF crystals.

As seen in the EDX mapping analysis (Fig. 4), all elements such as carbon, nitrogen, oxygen, and chromium have a uniform distribution on the surface of MIL-101(Cr)-30. These Chemical compounds emphasize the validity of the synthesis method using magnetized deionized water

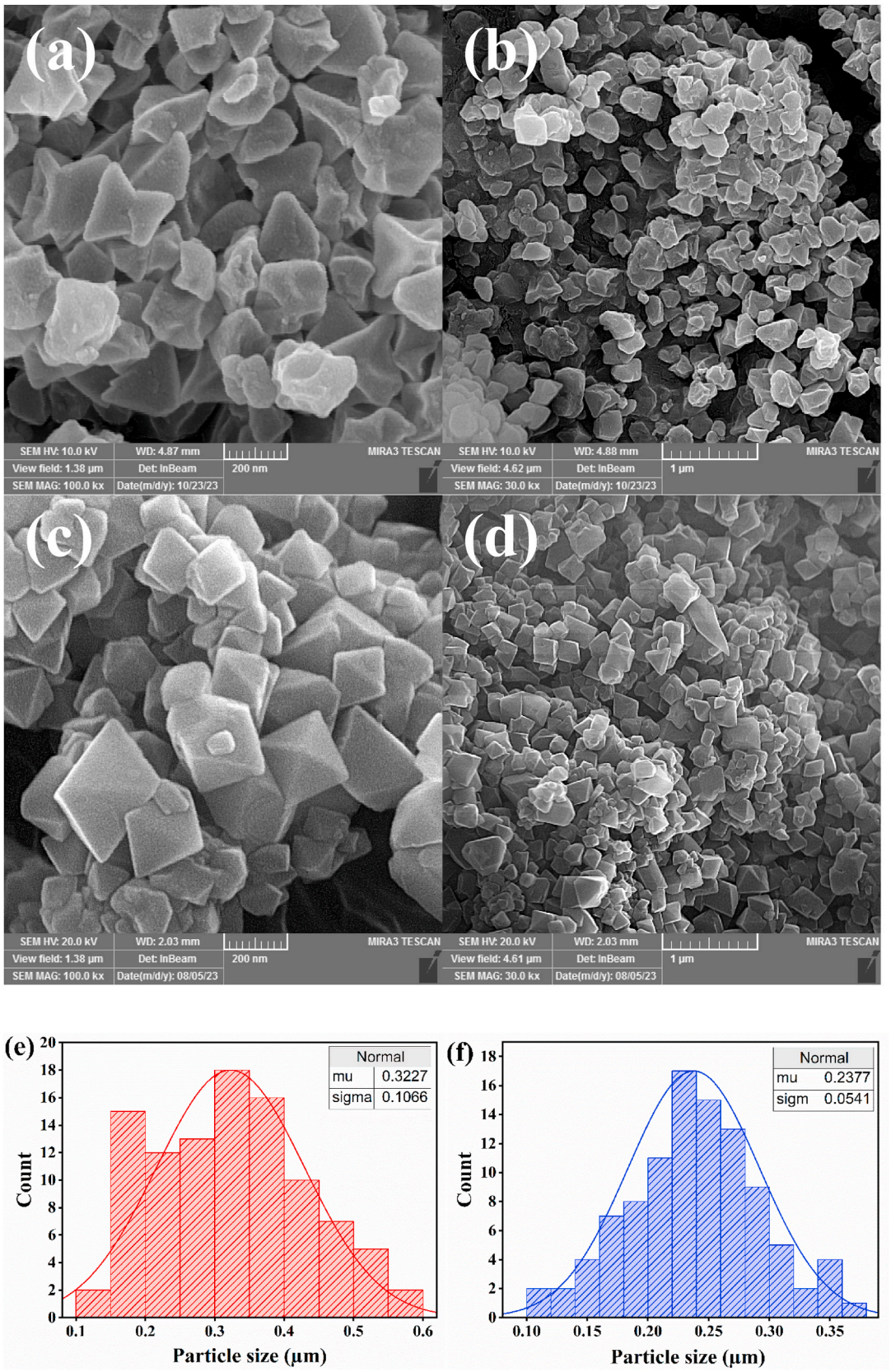


**Fig. 3.** FESEM images of: (a, b) MIL-101(Cr)-0 and (c, d) MIL-101(Cr)-30; (e, f) Particle size distribution of MIL-101(Cr)-0 and MIL-101(Cr)-30.

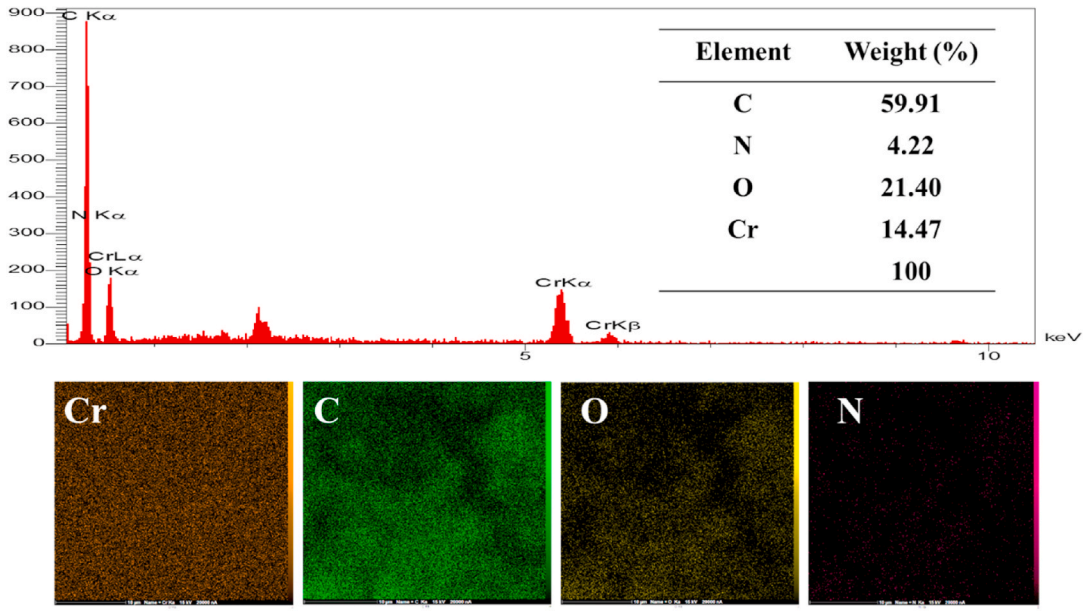


**Fig. 4.** EDX spectra and related elemental distribution maps of MIL-101(Cr)-30.

as a solvent [60].

Fig. 5 indicates the $N_2$ adsorption-desorption and distribution of the synthesized MIL-101(Cr) pore size determined at 77 K. MIL-101(Cr)-0 revealed a type I and mostly microporous, while a type IV isotherm featuring a hysteresis loop upon desorption appeared for MIL-101(Cr)-30 with a combination of mesopores and micropores. Type H1 hysteresis is shown according to the IUPAC classification. Two uptake steps at low relative pressures, around 0.1 and 0.2, indicate the two types of pore cages in the structures [59,60].

The textural characteristics of the synthesized samples are reported in Table 4. The surface area of MIL-101(Cr)-30 is approximately 3257 $m^2\ g^{-1}$, which is exceeding 2821 $m^2\ g^{-1}$ for MIL-101(Cr)-0. The average pore diameter ($d_P$) for MIL-101(Cr)-0 and MIL-101(Cr)-30 was 2.12 nm and 2.77 nm, respectively. The increase from 1.49 $cm^3\ g^{-1}$ to 2.26 $cm^3\ g^{-1}$ was observed for the pore volume ($V_p$) of MIL-101(Cr)-0 in comparison to MIL-101(Cr)-30. These results indicate that magnetized deionized water increases the porosity of MIL-101(Cr)-0 and improves the surface area of the adsorbent. Increasing the pore volume attributed to the more sustainable frameworks and recrystallized terephthalate linkers. The duration of exposure of the solvent to the magnetic field significantly affects crystal nucleation and growth by altering the behavior of water molecules and dissolved ions through changes in the hydrogen bonding network. An optimal magnetization period of 30 min encourages uniform crystal formation (as confirmed by FESEM results) and maximizes surface area. However, increasing this time to 60 min can disrupt the nucleation process, potentially causing excessive nucleation or smaller particle sizes. This can lead to particle agglomeration and loss of structural integrity, which may block pores and reduce the surface area from 3257 to 2634 $m^2\ g^{-1}$, as shown in Table 4.

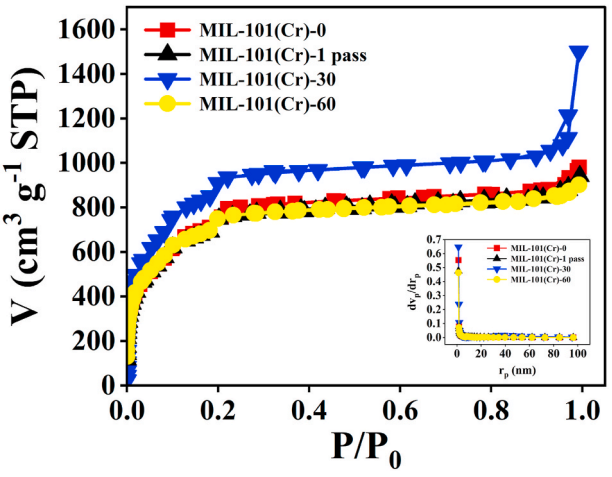


**Fig. 5.** $N_2$ adsorption-desorption isotherms and pore size distributions of MIL-101(Cr)-X (X: 0, 1 pass, 30, and 60).

**Table 4**
Results of BET analysis for treated MIL-101(Cr) and untreated MIL-101(Cr)-30.

| Adsorbent | $S_{BET}$ ($m^2\ g^{-1}$) | $V_p$ ($cm^3\ g^{-1}$) | $d_p$ (nm) |
|---|---|---|---|
| **MIL-101(Cr)-0** | 2821 | 1.49 | 2.12 |
| **MIL-101(Cr)-1 pass** | 2644 | 1.43 | 2.17 |
| **MIL-101(Cr)-30** | 3257 | 2.26 | 2.77 |
| **MIL-101(Cr)-60** | 2634 | 1.38 | 2.10 |

### 3.4. Formation mechanism

Water molecules are diamagnetic, meaning they have no unpaired electrons and no permanent magnetic moments. When exposed to an external magnetic field, they produce small opposing magnetic fields due to the circulation of electron currents. This diamagnetic response causes molecules to be repelled by the external field, resulting in subtle but significant changes in their behavior [61,62]. This interaction alters the hydrogen bonding within water clusters, affecting their stability, size, and network structure [63]. According to the collective findings from experimental research, magnetic field breaks or weakens the intra-cluster hydrogen bonds (HB) in water clusters, and after magnetization of water, more single water molecules with stronger inter-cluster hydrogen bonds are formed [64]. Reducing the size of clusters changes the molecular energy because the affinity of water for ions is enhanced as the activity of water increases [20]. This causes further ionization of water and the dissociation of impurities into positive and negative ions, enhancing the conductivity of liquid water [29,58]. Furthermore, these changes may affect the solubility behavior of ions (e.g., chromium ions) in the dissolution phase, potentially affecting the formation and stability of coordination complexes. The dynamic behavior of the hydrogen bond network in water exposed to a magnetic

field is described by the equation $(H_2O)_n \leftrightarrow x\,H_2O + (H_2O)_{n-x}$, with n-x indicating the formation of smaller water clusters [51]. The change induced by magnetized deionized water leads to increased molecular alignment and more uniform nucleation, which in turn improves crystal growth through better incorporation of terephthalic acid (BDC) with chromium ions. This process reduces structural defects and increases crystallinity. The plausible mechanism of MIL-101(Cr) formation follows these steps (Scheme 3): when the precursors, including chromium (III) nitrate nanohydrate ($Cr(NO_3)_3{\cdot}9H_2O$) and terephthalic acid ($H_2BDC$), are dissolved in magnetized water, chromium(III) ions ($Cr^{3+}$) undergo hydrolysis and form hydroxo complexes. During hydrolysis, terephthalic acid ($H_2BDC$) partially deprotonates to form terephthalate ions ($BDC^{2-}$) in the hydrolysis process. Coordination bonds are then formed between chromium cations and $BDC^{2-}$ anions, creating oligomeric clusters (coordination step). As these clusters further aggregate and grow into larger structures, nucleation occurs (nucleation step). Over time, these clusters transform into the distinct three-dimensional porous framework of MIL-101(Cr) [59,65,66]. In summary, water magnetization affects the formation of MIL-101(Cr) through three primary physicochemical pathways: (1) it modifies hydrogen bonding by reducing the size and stability of water clusters, thereby strengthening inter-cluster interactions and improving the distribution of reactants; (2) it increases the ion solvation by boosting the ionic mobility and solubility of precursor ions such as $Cr^{3+}$, which leads to faster and more homogeneous coordination processes; and (3) it accelerates nucleation kinetics by improving molecular orientation and increasing the reaction rates, leading to more stable crystal growth. Collectively, these factors contribute to greater crystallinity and higher surface area, as shown by XRD and BET results.

## 4. Statistical analysis

Based on the response surface method, the reduced quartic was the best-fitted model for predicting the influence of independent variables, including pH, contact time, and adsorbent dose, on IBP removal. The adsorption capacity of IBP ($q_e$, mg $g^{-1}$) was ascertained using the following coded equation (Eq. (5)):

$$q_e = 75.62 - 3.76A + 6.53B - 25.25C + 6.51AB + 2.99AC - 8.92BC - 11.32A^2 + 0.17B^2 + 4.67C^2 - 5.33ABC + 4.34A^2B - 14.03A^2C - 7.18AB^2 + 1576A^2B^2 \quad (5)$$

where A, B, and C are pH, contact time, and adsorbent dose.

Table 5 represents all 34 runs with six central points and two replicates for both factorial and axial points. All these measures are to minimize experimental errors.

ANOVA results of IBP removal by MIL-101(Cr)-30 are reported in Table 6. According to the results, a high F-value equal to 206.73 and a p-value <0.0001 indicate a significant model. Parameters with a P-value greater than 0.5 are insignificant, and those with a P-value less than 0.0001 are significant [49]. The adjusted and predicted R-squared values for the reduced quartic model were 0.9887 and 0.9745, respectively. These values demonstrated the accuracy of the predicted model for the available data. It is worth mentioning that the coefficient of variance was below 10 (CV = 4.84 %) and emphasized the experimental data without scattering to the predicted data. The signal-to-noise ratio, estimated by adequate precision, is 44.3588. This value exceeds 4 and is considered desirable [67,68].

Fig. 6a illustrates that the predicted values closely match the actual values, emphasizing the accuracy of the model. According to Fig. 6b, the normal plot of the residuals showed a normal data distribution with a regular scattering along a straight line.

### 4.1. Effect of variables

The response surface plots of IBP elimination by synthesized MIL-101 (Cr)-30 are presented in Fig. 6c and d. As can be seen in Fig. 6c, the interaction effect of time and adsorbent dose is effective in the removal experiments. The maximum amount of IBP removal was obtained in the 30 min interaction of 0.125 g $L^{-1}$ of MIL-101(Cr)-30 with the pollutant. A large percentage of removal occurred during the intermediate times of the adsorbent process. Because of accessible sites on the surface, increasing the adsorbent dose increased the removal efficiency. The high surface area and pore volume of MIL-101(Cr)-30 lead to excellent removal even at low amounts of adsorbent, introducing the synthesized

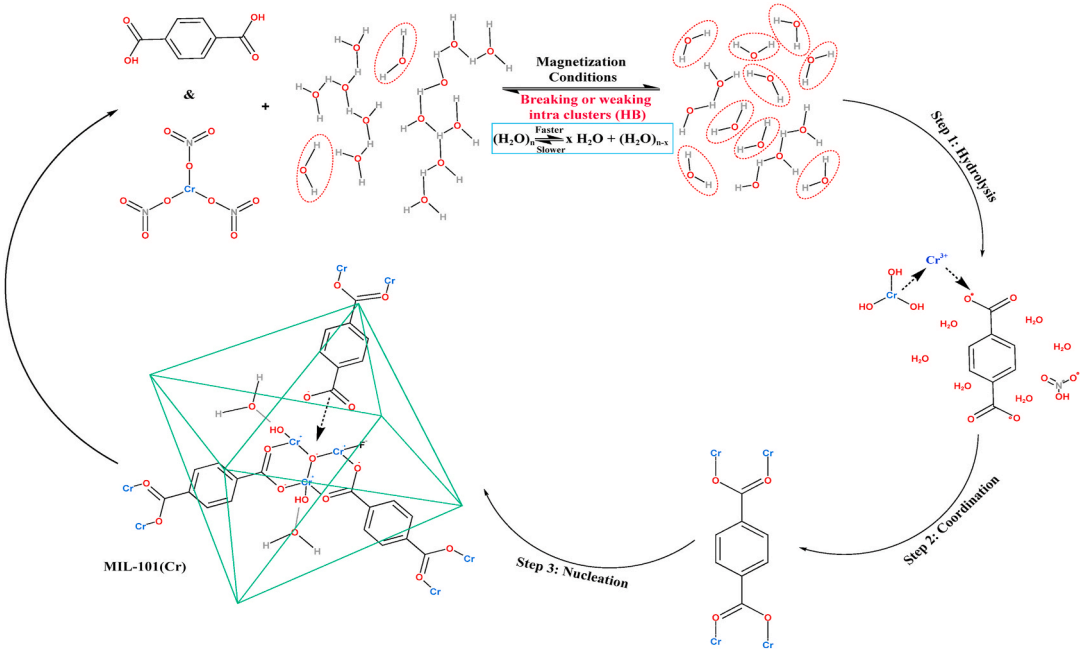


**Scheme 3.** Plausible mechanism of MIL-101(Cr) formation using Magnetized water.

**Table 5**
Independent variables and experimental data of IBP removal by MIL-101(Cr)-30.

| No. of experiment | Type | A: pH | B: Contact Time (min) | C: Adsorbent Dose (g $L^{-1}$) | Efficiency (%) | Adsorption capacity (mg $g^{-1}$) |
|---|---|---|---|---|---|---|
| 1 | Center | 6 | 20 | 0.1375 | 81 | 76.95 |
| 2 | Factorial | 4 | 30 | 0.2125 | 88 | 53.83 |
| 3 | Factorial | 4 | 10 | 0.2125 | 81 | 49.79 |
| 4 | Axial | 6 | 20 | 0.0250 | 23 | 121.2 |
| 5 | Factorial | 8 | 10 | 0.2125 | 56 | 34.35 |
| 6 | Axial | 6 | 5 | 0.1375 | 70 | 64.29 |
| 7 | Factorial | 8 | 30 | 0.2125 | 61 | 37.36 |
| 8 | Factorial | 8 | 10 | 0.2125 | 59 | 34.73 |
| 9 | Axial | 6 | 20 | 0.2500 | 94 | 49 |
| 10 | Axial | 9 | 20 | 0.1375 | 51 | 36.29 |
| 11 | Axial | 9 | 20 | 0.1375 | 56 | 52.73 |
| 12 | Axial | 3 | 20 | 0.1375 | 61 | 57.67 |
| 13 | Factorial | 4 | 30 | 0.0625 | 72 | 150.4 |
| 14 | Factorial | 8 | 30 | 0.2125 | 72 | 44.28 |
| 15 | Factorial | 4 | 30 | 0.0625 | 68 | 141.76 |
| 16 | Center | 6 | 20 | 0.1375 | 78 | 74.18 |
| 17 | Factorial | 8 | 30 | 0.0625 | 67 | 139.84 |
| 18 | Center | 6 | 20 | 0.1375 | 78 | 74.18 |
| 19 | Center | 6 | 20 | 0.1375 | 82 | 77.38 |
| 20 | Factorial | 8 | 10 | 0.0625 | 39 | 80.32 |
| 21 | Factorial | 8 | 30 | 0.0625 | 69 | 144 |
| 22 | Axial | 6 | 20 | 0.2500 | 90 | 47.48 |
| 23 | Axial | 6 | 5 | 0.1375 | 71 | 68.14 |
| 24 | Axial | 3 | 20 | 0.1375 | 57 | 53.89 |
| 25 | Axial | 6 | 35 | 0.1375 | 89 | 85.38 |
| 26 | Axial | 6 | 20 | 0.0250 | 24 | 126.8 |
| 27 | Factorial | 4 | 10 | 0.2125 | 91 | 55.82 |
| 28 | Center | 6 | 20 | 0.1375 | 79 | 75.05 |
| 29 | Center | 6 | 20 | 0.1375 | 80 | 76 |
| 30 | Factorial | 4 | 10 | 0.0625 | 62 | 129.28 |
| 31 | Factorial | 4 | 30 | 0.2125 | 89 | 54.87 |
| 32 | Factorial | 8 | 10 | 0.0625 | 37 | 76.96 |
| 33 | Factorial | 4 | 10 | 0.0625 | 63 | 131.04 |
| 34 | Axial | 6 | 35 | 0.1375 | 91 | 86.25 |

**Table 6**
ANOVA results of IBP removal on MIL-101(Cr)-30 model.

| Source | Sum of squares | df | Mean square | F-value | p-value | |
|---|---|---|---|---|---|---|
| **Model** | 41479.02 | 14 | 2962.79 | 206.73 | <0.0001 | Significant |
| A-pH | 127.01 | 1 | 127.01 | 8.86 | 0.0077 | |
| B-Time | 384.16 | 1 | 384.16 | 26.81 | <0.0001 | |
| C-Adsorbent Dose | 5739.58 | 1 | 5739.58 | 400.49 | <0.0001 | |
| AB | 678.47 | 1 | 678.47 | 47.34 | <0.0001 | |
| AC | 142.62 | 1 | 142.62 | 9.95 | 0.0052 | |
| BC | 1273.60 | 1 | 1273.60 | 88.87 | <0.0001 | |
| $A^2$ | 1557.95 | 1 | 1557.95 | 108.71 | <0.0001 | |
| $B^2$ | 0.3682 | 1 | 0.3682 | 0.0257 | 0.8744 | |
| $C^2$ | 264.43 | 1 | 264.43 | 18.45 | 0.0004 | |
| ABC | 454.22 | 1 | 454.22 | 31.69 | <0.0001 | |
| $A^2B$ | 108.73 | 1 | 108.73 | 7.59 | 0.0126 | |
| $A^2C$ | 1134.17 | 1 | 1134.17 | 79.14 | <0.0001 | |
| $AB^2$ | 296.75 | 1 | 296.75 | 20.71 | 0.0002 | |
| $A^2B^2$ | 1085.96 | 1 | 1085.96 | 75.77 | <0.0001 | |
| **Pure Error** | 272.30 | 19 | 14.33 | | | |
| **Cor Total** | 41751.32 | 33 | | | | |

MOF for industrial and large-scale applications. Also, the removal efficiency of pollutants improves by increasing the exposure time. As a result, contact time and adsorbent dose variables directly correlate with the removal efficiency of IBP on MIL-101(Cr)-30. The relationship between pH and adsorbent dose in the treatment process is shown in Fig. 6d. It is clear that the maximum removal value was attained at acidic pH (4–6) and 0.125 g $L^{-1}$ adsorbent. These variables have an indirect relationship compared to the removal value. Adsorption capacity varies with changes, which is due to surface charge and functional groups. The potential of zeta analysis of MIL-101(Cr)-30 under varying pH levels is shown in Fig. 7, and the $pH_{pzc}$ is almost 4.6. The positive charge of the MIL-101(Cr)-30 surface happens when the pH of the solution is below 4.6, and the negative charge is when the pH of the solution is above 4.6. In other words, the structure of MIL-101(Cr)-30 is protonated in acidic solutions and vice versa in basic solutions. It should be noted that the pKa of ibuprofen is 4.9, and the carboxylic acid group acts as a hydrogen acceptor at pH < 4.9 and as a hydrogen donor at pH > 4.9 [69]. Therefore, under an acidic pH range, especially between 4.5 and 5, electrostatic interaction occurs between IBP molecules and adsorbent sites. Hydrogen bonding and π-π interaction among the benzene rings of MIL-101(Cr)-30 and the aromatic rings of ibuprofen increased the efficiency of the adsorbent [55]. On the other hand, the repulsive forces created at basic pH reduced the removal efficiency due to the anionic form of IBP and the negative surface of MIL-101(Cr)-30.

Typically, zeta potential measurements taken at varying exposure times revealed the influence of the magnetic field on surface charge

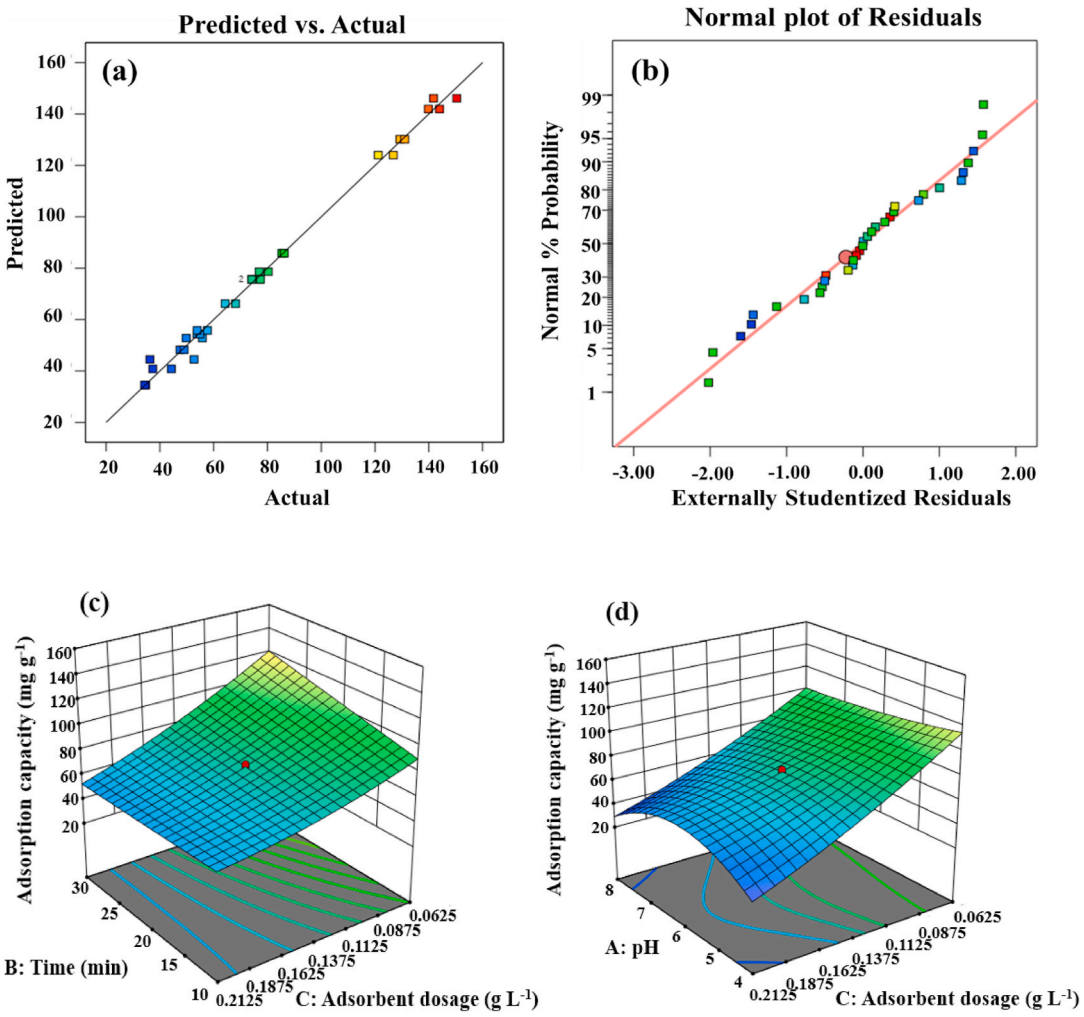


**Fig. 6.** (a) Predicted vs. actual value; (b) Normal plot of residuals for IBP adsorption by the MIL-101(Cr)-30; (c, d) 3D interaction plots of time vs. adsorbent dose and pH vs. adsorbent dose.

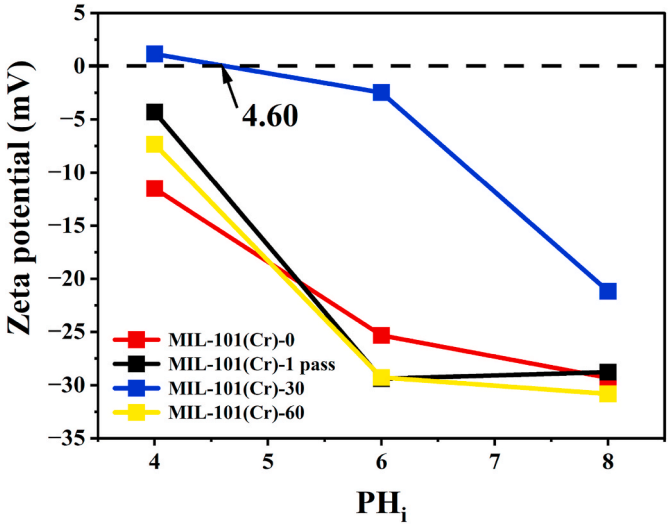


**Fig. 7.** Zeta potential of MIL-101(Cr)-X (X: 0, 1 pass, 30, and 60) at different pH values.

(Fig. 7). The impact of magnetized water on the zeta potential of adsorbents can be due to alterations in the arrangement of charged particles or ions within the structure. This could potentially influence the electrostatic interactions between particles and their surroundings, depending on the conditions. Various studies have shown that the magnetic field significantly influences the zeta potential, and it was commonly believed that the Lorentz forces $\vec{F} = q.\vec{v} \times \vec{B}$ acted on either moving ions or charged solid particles [32,50], with Madsen proposing that the magnetic field affected proton spin [70].

### 4.2. Optimization

The influence of operating conditions and removal efficiency was optimized using CCD-RSM design, and Table 7 presents the optimal conditions. Due to the importance of pH and adsorbent dose, consider pH values of 4.5 and adsorbent dose in the medium range (0.1375 g $L^{-1}$) to obtain the maximum removal efficiency. Adsorption time and capacity are within limits. The best optimized results were suggested pH 4.5, contact time 30 min, and adsorbent dose 0.125 g $L^{-1}$. The removal efficiency was approximately 90 %, and the adsorption capacity was 90.59 mg $g^{-1}$ under optimal conditions with a desirability of 0.976. The experiment was repeated in real conditions to confirm the correctness of the predicted values. The actual removal efficiency of 90.41 % and the actual adsorption capacity of 92.47 mg $g^{-1}$ emphasized the accuracy of the model prediction. The parent MIL-101(Cr)-0 had a yield of removal

**Table 7**
Optimal operating conditions and predicted removal amount.

| pH | Time (min) | Adsorbent Dose (g $L^{-1}$) | Removal efficiency (%) | Adsorption capacity (mg $g^{-1}$) | Desirability | |
|---|---|---|---|---|---|---|
| 4.5 | 30.000 | 0.125 | 90 | 90.59 | 0.976 | **Selected** |

of 74.96 % and adsorption capacity of 76.67 mg $g^{-1}$ under these optimal conditions. Therefore, MIL-101(Cr)-30 showed better performance in water treatment compared to MIL-101(Cr)-0.

## 5. Kinetic study

The adsorption rate and the effect of exposure time on the IBP elimination by the prepared MOF are presented in Fig. 8a and b. The adsorbent-adsorbate interaction was carried out on ibuprofen solution (10 mg $L^{-1}$) under the following conditions: pH = 4.5, adsorbent dose = 0.125 g $L^{-1}$, volume = 40 $cm^3$. Fig. 8a demonstrates that the adsorption rate rapidly increased during the first 20 min and then gradually decreased until equilibrium was reached. Over time, occupation of active sites and reduction of exposed surface lead to a reduction in interaction between IBP molecules and adsorbent, which in turn slows down the adsorption rate. Additionally, the adsorption kinetic activities between the IBP and MIL-101(Cr)-30 were evaluated using two kinetic models, pseudo-first-order (Lagergren) and pseudo-second-order (Ho). The experimental data fitting is illustrated in Fig. 8b. The equations of Lagergren and Ho [71,72] are detailed as follows (Eqs. (6) and (7)):

Pseudo-first-order model:

$$Log(q_e - q_t) = Log(q_e) - \frac{k_1 t}{2.303} \quad (6)$$

$q_t$ (mg $g^{-1}$) and $q_e$ (mg $g^{-1}$) are the adsorption capacity of IBP at each time (t) and equilibrium, respectively. $k_1$ ($min^{-1}$) is the pseudo-first-order kinetic constant.

Pseudo-second-order model:

$$\frac{t}{q_t} = \frac{1}{k_2 q_e^2} + \frac{t}{q_e} \quad (7)$$

where $k_2$ (g $mg^{-1}$ $min^{-1}$) denotes the rate constant for pseudo-second-order kinetic.

Kinetic parameters and correlation coefficients ($R^2$) obtained from each model for IBP removal by MIL-101(Cr)-30 are presented in Table 8. The findings showed that the pseudo-second-order model most accurately matched the observational data, as it exhibited the highest correlation coefficient of the models ($R^2$ = 0.99). Consequently, the adsorption of IBP occurs through rapid diffusion chemisorption, involving electrostatic and π-π interactions among the pollutant molecules and adsorbent [71,73].

**Table 8**
Kinetic parameters of IBP adsorption on MIL-101(Cr)-30.

| pseudo-first-order model | | | pseudo-second-order model | | |
|---|---|---|---|---|---|
| $k_1$ ($min^{-1}$) | $q_e$ (mg $g^{-1}$) | $R^2$ | $k_2$ (g $mg^{-1}$ $min^{-1}$) | $q_e$ (mg $g^{-1}$) | $R^2$ |
| 0.314 | 101.578 | 0.804 | 0.0018 | 81.967 | 0.987 |

## 6. Isotherm study

The diffusion and distribution of IBP molecules within the pores of the adsorbent at adsorption equilibrium were characterized using two adsorption isotherm models: The Freundlich and Langmuir. Different

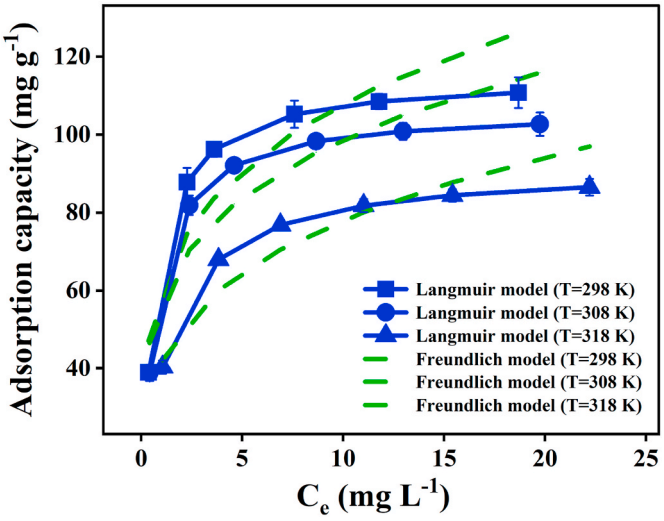


**Fig. 9.** Adsorption isotherms fitted to the Langmuir model and the Freundlich model for adsorption of IBP on MIL-101(Cr)-30 (conditions: pH = 4.5, contact time = 30 min, and adsorbent dose = 0.125 g $L^{-1}$).

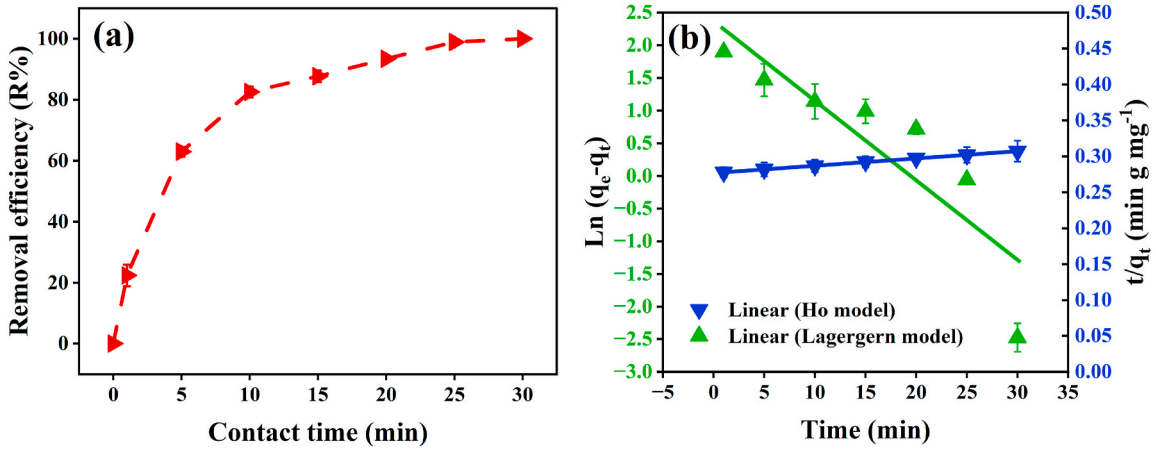


**Fig. 8.** (a) Removal efficiency of ibuprofen by MIL-101(Cr)-30 versus contact time; (b) Fitted pseudo-first-order and pseudo-second-order models for adsorption of IBP on MIL-101(Cr)-30.

initial concentrations of ibuprofen solution (5, 10, 15, 20, 25, and 30 mg $L^{-1}$) and temperatures (298, 308, and 318 K) were collected for these studies and the adsorption isotherm curves of these models to fit the experimental data were represented in Fig. 9. It should be noted that all experiments were performed under optimal conditions for 40 $cm^3$ ibuprofen solution. The results indicated that an exothermic process occurred during the removal reaction by the decrease in the adsorption efficiency of IBP with increasing temperature. Freundlich and Langmuir equations [71,73] are detailed as follows (Eqs. (8) and (9)):

Freundlich model:

$$q_e = K_F.C_e^{\frac{1}{n}} \tag{8}$$

$K_F$ ($L.g^{-1}$) is a constant and relative indicator of Freundlich adsorption capability. 1/n is the adsorption energy of IBP. $q_e$ and $C_e$ are the equilibrium adsorption capability and the equilibrium concentration of IBP, respectively.

Langmuir model:

$$q_e = \frac{q_m.K_L.C_e}{1 + K_L.C_e} \tag{9}$$

$K_L$ ($L.g^{-1}$) and $q_m$ are the Langmuir constant and the maximum capability of MIL-101(Cr)-30 for IBP removal.

Adsorption isotherm parameters of IBP on MIL-101(Cr)-30 obtained from each model are presented in Table 9. The Langmuir parameters exhibited a superior fit with the data, and high correlation coefficients ($R^2$ = 0.9988, 0.9996, and 0.9994) at each temperature, compared to the Freundlich ($R^2$ = 0.8956, 0.9097, and 0.8956). Therefore, the adsorption isotherm data for IBP adsorption aligned with the Langmuir isotherm model, indicating homogeneous adsorption of IBP on a uniform monolayer surface of MIL-101-30. In addition, the parameter n in the Freundlich isotherm is greater than 1, suggesting a uniform adsorbent surface, which is consistent with the assumptions of the Langmuir model [71].

## 7. Thermodynamic study

The relationship between temperature and rate of IBP diffusion into the adsorbent pores was investigated using enthalpy (ΔH, kJ $mol^{-1}$), entropy (ΔS, J $mol^{-1}$ $K^{-1}$), and Gibbs free energy (ΔG, kJ $mol^{-1}$), mentioned as thermodynamic parameters. The impact of temperature on the IBP elimination by MIL-101(Cr)-30 was evident at 298, 308, and 318 K, respectively (Fig. 10a). Gibbs free energy is calculated by Eq. (10). The values of enthalpy and entropy are acquired from the Van't Hoff (Eq. (11)) [71], the curve of $LnK_0$ vs. 1/T is plotted in Fig. 10b.

$$\Delta G = -RTLnK \tag{10}$$

$$LnK = \frac{\Delta S}{R} - \frac{\Delta H}{RT} \tag{11}$$

in the above equations, K represents the equilibrium adsorption constant, T (k) represents the temperature of the solution, and R (8.314 J $mol^{-1}$ $k^{-1}$) is the ideal gas constant.

The thermodynamic data are detailed in Table 10. The negative ΔG values at all temperatures indicate that the IBP molecules were adsorbed spontaneously on MIL-101(Cr)-30 and are thermodynamically feasible. moreover, the less negative ΔG values (from −4.462 to −3.670 kJ $mol^{-1}$) with increasing temperature (298–318 K) suggest that the favorable adsorption reaction occurs at lower temperatures. The adsorption process was exothermic based on the negative value of enthalpy (ΔH). Additionally, the negative value of entropy (ΔS) indicated less disorder and randomness within the reaction system [4,71].

**Table 9**
Adsorption isotherm parameters of IBP on MIL-101(Cr)-30.

| T (K) | Langmuir model | | | Freundlich model | | | |
|---|---|---|---|---|---|---|---|
| | $K_L$ (L $g^{-1}$) | $q_m$ (mg $g^{-1}$) | $R^2$ | $K_F$ (L $g^{-1}$) | $q_e$ (mg $g^{-1}$) | n | $R^2$ |
| 298 | 1.426 | 114.942 | 0.998 | 60.782 | 109.85 | 4.008 | 0.895 |
| 308 | 1.403 | 106.382 | 0.999 | 57.414 | 102.71 | 4.248 | 0.909 |
| 318 | 0.746 | 91.743 | 0.999 | 41.633 | 86.25 | 3.668 | 0.895 |

## 8. Regeneration of adsorbent

Reusing adsorbents is a crucial strategy in adsorption processes, particularly for industrial applications. Therefore, the reusability of MIL-101(Cr)-30 was considered to remove IBP from aqueous medium by centrifugation. The IBP molecules trapped in the pores of the adsorbent were released by mixing with 100 $cm^3$ ethanol solution (99 %, Merck) for 1 h, resulting in electrostatic repulsions between IBP and MIL-101 (Cr)-30. Fig. 11 illustrates the performance of the synthesized MIL-101 (Cr) over five recycling cycles, demonstrating its potential for large-scale applications. The slight difference between the first and fifth regeneration cycles may be due to the wastage of the adsorbent during washing.

## 9. Comparison of synthesis conditions and textural properties

A comparative study of the synthesis conditions and textural properties of the MIL-101(Cr) adsorbent, as detailed in recent publications, is presented in Table 11. In our study, magnetized deionized water (MDW) was employed as a synergistic solvent, significantly contributing to the development of a highly porous and stable framework. The enhanced BET surface area (3257 $m^2$ $g^{-1}$) and large total pore volume are attributed to improved molecular alignment and more uniform nucleation, which likely reduced structural defects and increased crystallinity. The solvent in the synthesis of MIL-101(Cr) plays a crucial role in dissolving the reactants and facilitating the formation of the metal-organic framework. As discussed in the FESEM analysis, MDW appears to increase the nucleation rate of MOF cores and promote the formation of well-defined octahedral crystals. This higher nucleation rate distributes the starting materials to more nucleation sites, limiting the growth of individual crystals and resulting in smaller particle sizes. Furthermore, during the washing steps, any unreacted material or excess solvent is removed from the rigid framework of MOFs. The interaction and arrangement of terephthalic acid (BDC) with chromium ions may change when using magnetized deionized water (MDW), potentially affecting the connectivity of the framework and enhancing the purification process.

## 10. Conclusion

MIL-101(Cr) adsorbents were successfully synthesized by modifying them with magnetized deionized water using hydrothermal methods, and their adsorption behavior in removing IBP was investigated. The structures and properties of the prepared MOF were identified by employing XRD, FTIR, FESEM, EDX, BET, BJH, and zeta potential analysis. The synthesized MIL-101(Cr) revealed uniform octahedral crystals with a high BET surface area of approximately 3257 $m^2$ $g^{-1}$, a total pore volume of 2.26 $cm^3$ $g^{-1}$, and a pore diameter of 2.77 nm. Based on the CCD results conducted to identify the optimal parameters, the interaction between the independent variables significantly impacted the removal efficiency. A reduced quartic model with an adjusted R-squared of 0.9887 is suitable for modeling the data. Under optimal conditions, MIL-101(Cr)-30 achieved a maximum adsorption capacity of 92.47 mg $g^{-1}$ for IBP, with a removal efficiency of 90.41 %. Additionally, the MIL-101(Cr) treated with 30 min magnetized water exhibited up to a 15 % higher removal efficiency compared to the unmodified MIL-101(Cr), which can be attributed to its increased surface area and the shift in the $pH_{pzc}$ point resulting from the use of magnetized

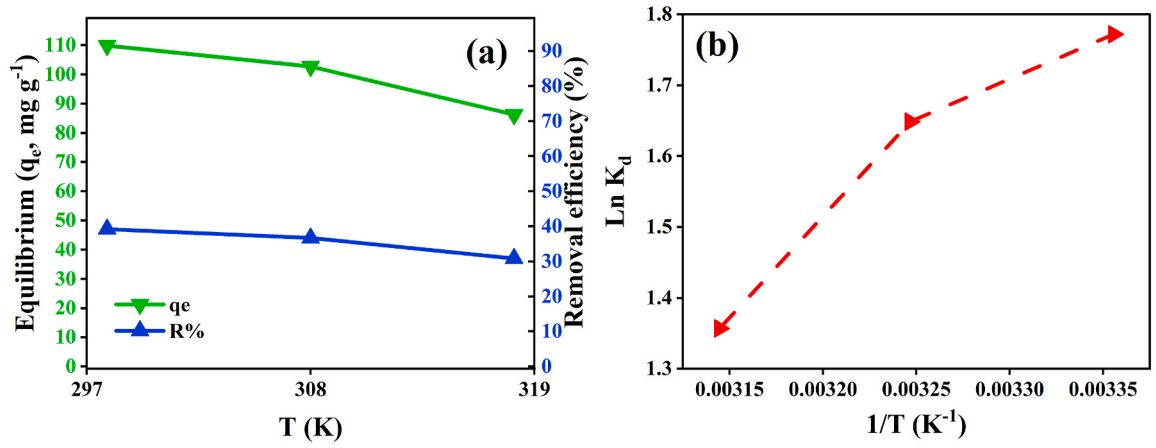


**Fig. 10.** (a) Removal efficiency of IBP by MIL-101(Cr)-30 versus temperature; (b) Thermodynamic diagram (conditions: pH = 4.5, contact time = 30 min, and adsorbent dose = 0.125 g $L^{-1}$).

**Table 10**
Thermodynamic parameters of IBP on MIL-101(Cr)-30.

| T (K) | ΔG (kJ $mol^{-1}$) | ΔH (kJ $mol^{-1}$) | ΔS (J $mol^{-1}$ $K^{-1}$) |
|---|---|---|---|
| 298 | −4.462 | −16.268 | −39.618 |
| 308 | −4.066 | | |
| 318 | −3.670 | | |

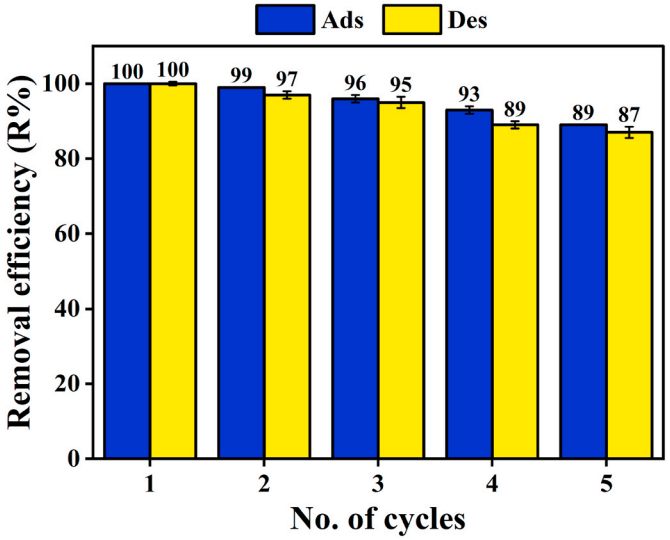


**Fig. 11.** Reusability of MIL-101(Cr)-30 in different cycle numbers.

water during synthesis. Additionally, the adsorption of IBP on MIL-101 (Cr)-30 is predicted to follow monolayer chemisorption, as indicated by the Ho kinetic and the Langmuir isotherm model. The reusable experiments of MIL-101(Cr)-30 showed an 11 % decrease in removal efficiency after five cycles of regeneration using an ethanol solution as a desorption agent. According to the findings of this study, magnetized deionized water as an eco-friendly and user-friendly solvent influences the morphology and crystal structure of MIL-101(Cr), which is useful for increasing the adsorption capacity of this adsorbent. Consequently, we are now interested in further investigating the use of this solvent for synthesizing nanostructures in our laboratory.

## CRediT authorship contribution statement

**Sara Abolhasani:** Writing – original draft, Visualization, Validation,

**Table 11**
Comparison of prepared MIL-101(Cr) with other recently reported MIL-101(Cr) adsorbents.

| Adsorbent | Synthesis conditions | | Textural properties | | | Ref |
|---|---|---|---|---|---|---|
| | Medium | Purification | $S_{BET}$ ($m^2$ $g^{-1}$) | $V_p$ ($cm^3$ $g^{-1}$) | $d_p$ (nm) | |
| MIL-101 (Cr) | $H_2O$/HF | EtOH/DMF/ $NH_4F$/Hot $H_2O$ | 3323.27 | 1.71 | – | [74] |
| MIL-101 (Cr) | $H_2O$/HF | DMF/Hot EtOH | 3311.88 | 1.57 | – | [71] |
| MIL-101 (Cr) | $H_2O$/HF | $H_2O$/DMF/ EtOH | 2351.78 | – | 2.01 | [8] |
| MIL-101 (Cr) | $H_2O$/HF | $H_2O$ | 1085.85 | – | 2.3 | [75] |
| MIL-101 (Cr) | $H_2O$/$HNO_3$ | Hot DMF/ EtOH/$H_2O$ | 3431 | 1.68 | – | [54] |
| MIL-101 (Cr) | H2O/AcOH | Hot $H_2O$/ DMF/EtOH | 1372.4 | – | – | [76] |
| MIL-101 (Cr) | $H_2O$ | Hot EtOH/ $H_2O$/Ace | 2134 | 1.15 | 1.61 | [77] |
| MIL-101 (Cr) | $H_2O$ | EtOH | 2592.2 | 1.09 | – | [47] |
| MIL-101 (Cr) | $H_2O$ | Not reported | 2997 | 1.48 | 2.18 | [78] |
| MIL-101 (Cr)-0 | $H_2O$/AcOH | $H_2O$/DMF/ EtOH/$NH_4F$ | 2821 | 1.49 | 2.12 | **This work** |
| MIL-101 (Cr)-30 | Magnetized $H_2O$/AcOH | $H_2O$/DMF/ EtOH and $NH_4F$ | 3257 | 2.26 | 2.77 | **This work** |
| MIL-101 (Cr)-0 | $H_2O$/AcOH | Hot $H_2O$/ DMF/EtOH and $NH_4F$ | 2643.9 | 1.43 | 2.17 | **This work** |
| MIL-101 (Cr)-30 | Magnetized $H_2O$/AcOH | Hot $H_2O$/ DMF/EtOH and $NH_4F$ | 3989.7 | 3.05 | 3.06 | **This work** |

Resources, Investigation, Formal analysis, Data curation. **Ali Ahmadpour:** Writing – review & editing, Supervision, Project administration, Conceptualization. **Mostafa Gholizadeh:** Writing – review & editing, Supervision, Conceptualization.

## Declaration of competing interest

The authors declare that they have no known competing financial interests or personal relationships that could have appeared to influence the work reported in this paper.

## Acknowledgments

The authors appreciate the support of Ferdowsi University of Mashhad, Iran (Grant No. 61392) for this work.

## Data availability

Data will be made available on request.

## References

[1] T. Xing, Y. Wu, Q. Wang, A. Sadrnia, A. Behmaneshfar, E.N. Dragoi, Adsorption of ibuprofen using waste coffee derived carbon architecture: experimental, kinetic modeling, statistical and bio-inspired optimization, Environ. Res. 231 (2023) 116223, https://doi.org/10.1016/j.envres.2023.116223.

[2] A.I. Osman, A. Ayati, M. Farghali, P. Krivoshapkin, B. Tanhaei, H. Karimi-Maleh, E. Krivoshapkina, P. Taheri, C. Tracey, A. Al-Fatesh, I. Ihara, D.W. Rooney, M. Sillanpaä, Advanced Adsorbents for Ibuprofen Removal from Aquatic Environments: a Review, Springer International Publishing, 2024, https://doi.org/10.1007/s10311-023-01647-6.

[3] A. Mojiri, M.J.K. Bashir, Wastewater treatment: current and future techniques, Water (Switzerland) 14 (2022) 10–12, https://doi.org/10.3390/w14030448.

[4] N.D. Alkhathami, N.A. Alamrani, A. Hameed, S.D. Al-Qahtani, R. Shah, N.M. El-Metwaly, Adsorption of pharmaceutical ibuprofen over functionalized zirconium metal-organic frameworks; batch experiment and mechanism of interaction, Polyhedron 235 (2023), https://doi.org/10.1016/j.poly.2023.116349.

[5] S. Abolhasani, A. Ahmadpour, T. Rohani Bastami, A. Yaqubzadeh, Facile synthesis of mesoporous carbon aerogel for the removal of ibuprofen from aqueous solution by central composite experimental design (CCD), J. Mol. Liq. 281 (2019) 261–268, https://doi.org/10.1016/j.molliq.2019.02.084.

[6] F. Ghiasi, A.R. Solaimany Nazar, M. Farhadian, S. Tangestaninejad, N. Emami, Synthesis of aqueous media stable MIL101-OH/chitosan for diphenhydramine and metronidazole adsorption, Environ. Sci. Pollut. Res. 29 (2022) 24286–24297, https://doi.org/10.1007/s11356-021-17739-1.

[7] H. Zhao, Q. Li, Z. Wang, T. Wu, M. Zhang, Synthesis of MIL-101(Cr) and its water adsorption performance, Microporous Mesoporous Mater. 297 (2020) 110044, https://doi.org/10.1016/j.micromeso.2020.110044.

[8] Q. Zhou, G. Liu, Urea-functionalized MIL-101(Cr)@AC as a new adsorbent to remove sulfacetamide in wastewater treatment, Ind. Eng. Chem. Res. 59 (2020) 12056–12064, https://doi.org/10.1021/acs.iecr.0c01037.

[9] Y. Yang, X. Li, Y. Gu, H. Lin, B. Jie, Q. Zhang, X. Zhang, Adsorption property of fluoride in water by metal organic framework: optimization of the process by response surface methodology technique, Surf. Interfaces 28 (2022) 101649, https://doi.org/10.1016/j.surfin.2021.101649.

[10] A. Jalali, A. Ahmadpour, M. Ghahramaninezhad, E. Yasari, Hierarchical nanocomposites derived from UiO-66 framework and zeolite for enhanced $CO_2$ adsorption, J. Environ. Chem. Eng. 11 (2023) 111294, https://doi.org/10.1016/j.jece.2023.111294.

[11] N.S. Abdul Mubarak, K.Y. Foo, R. Schneider, R.M. Abdelhameed, S. Sabar, The chemistry of MIL-125 based materials: structure, synthesis, modification strategies and photocatalytic applications, J. Environ. Chem. Eng. 10 (2022), https://doi.org/10.1016/j.jece.2021.106883.

[12] M. Shirkhodaie, S. Seidi, F. Shemirani, F. Zaroudi, Environmental contaminant analysis: concerns inspiring the emergence of MOF composites, TrAC - Trends Anal. Chem. 164 (2023) 117109, https://doi.org/10.1016/j.trac.2023.117109.

[13] C. Serre, F. Millange, G. Fe, A Chromium Terephthalate–Based Solid with Unusually Large Pore Volumes and Surface Area, 309, 2005.

[14] K. Adesina Adegoke, O. Samuel Agboola, J. Ogunmodede, A. Oluyomi Araoye, O. Solomon Bello, Metal-organic frameworks as adsorbents for sequestering organic pollutants from wastewater, Mater. Chem. Phys. 253 (2020) 123246, https://doi.org/10.1016/j.matchemphys.2020.123246.

[15] J. Wang, Y. Muhammad, Z. Gao, S. Jalil Shah, S. Nie, L. Kuang, Z. Zhao, Z. Qiao, Z. Zhao, Implanting polyethylene glycol into MIL-101(Cr) as hydrophobic barrier for enhancing toluene adsorption under highly humid environment, Chem. Eng. J. 404 (2021) 126562, https://doi.org/10.1016/j.cej.2020.126562.

[16] H.M.A. Hassan, M.A. Betiha, S.K. Mohamed, E.A. El-Sharkawy, E.A. Ahmed, Stable and recyclable MIL-101(Cr)–Ionic liquid based hybrid nanomaterials as heterogeneous catalyst, J. Mol. Liq. 236 (2017) 385–394, https://doi.org/10.1016/j.molliq.2017.04.034.

[17] M. Zou, M. Dong, T. Zhao, Advances in Metal-Organic Frameworks MIL-101 (Cr), 2022, p. 101.

[18] T. Hu, H. Lv, S. Shan, Q. Jia, H. Su, N. Tian, S. He, Porous structured MIL-101 synthesized with different mineralizers for adsorptive removal of oxytetracycline from aqueous solution, RSC Adv. 6 (2016) 73741–73747, https://doi.org/10.1039/c6ra11684a.

[19] T. Zhao, L. Yang, P. Feng, I. Gruber, C. Janiak, Y. Liu, Facile synthesis of nano-sized MIL-101(Cr) with the addition of acetic acid, Inorg. Chim. Acta. 471 (2018) 440–445, https://doi.org/10.1016/j.ica.2017.11.030.

[20] H. Rashidi, A. Ahmadpour, M. Gholizadeh, F.F. Bamoharram, F. Moosavi, Effect of magnetized ethanol on the shape evolution of zinc oxide from nanoparticles to microrods: experimental and molecular dynamic simulation study, Adv. Powder Technol. 29 (2018) 349–358, https://doi.org/10.1016/j.apt.2017.11.022.

[21] Z. Eshaghi, M. Gholizadeh, The effect of magnetic field on the stability of (18-crown-6) complexes with potassium ion, Talanta 64 (2004) 558–561, https://doi.org/10.1016/j.talanta.2004.02.039.

[22] M. Mousavi, A.N. Pour, M. Gholizadeh, Effect of "Magnetized Water" on size of nickel oxide nanoparticles and their catalytic properties in $CO_2$ reforming of methane, Theor. Exp. Chem. 55 (2020) 414–422, https://doi.org/10.1007/s11237-020-09634-6.

[23] N. Zhuo, Y. Lan, W. Yang, Z. Yang, X. Li, X. Zhou, Y. Liu, J. Shen, X. Zhang, Adsorption of three selected pharmaceuticals and personal care products (PPCPs) onto MIL-101(Cr)/natural polymer composite beads, Sep. Purif. Technol. 177 (2017) 272–280, https://doi.org/10.1016/j.seppur.2016.12.041.

[24] P.W. Seo, B.N. Bhadra, I. Ahmed, N.A. Khan, S.H. Jhung, Adsorptive removal of pharmaceuticals and personal care products from water with functionalized metal-organic frameworks: remarkable adsorbents with hydrogen-bonding abilities, Sci. Rep. 6 (2016) 1–11, https://doi.org/10.1038/srep34462.

[25] W. Sun, H. Li, H. Li, S. Li, X. Cao, Adsorption mechanisms of ibuprofen and naproxen to UiO-66 and UiO-66-$NH_2$: batch experiment and DFT calculation, Chem. Eng. J. 360 (2019) 645–653, https://doi.org/10.1016/j.cej.2018.12.021.

[26] A. Gilani, H. Kermanshahi, M. Gholizadeh, A. Golian, Agricultural water management through magnetization of irrigation water: a review, J. Arid. Agric. 3 (1970) 23–27, https://doi.org/10.25081/jaa.2017.v3.3353.

[27] A. Nakhaei Pour, M. Gholizadeh, M. Housaindokht, F. Moosavi, H. Monhemi, A new method for preparing mono-dispersed nanoparticles using magnetized water, Appl. Phys. A Mater. Sci. Process. 123 (2017), https://doi.org/10.1007/s00339-017-0876-7, 0.

[28] C. Sronsri, K. U-yen, W. Sittipol, Analyses of vibrational spectroscopy, thermal property and salt solubility of magnetized water, J. Mol. Liq. 323 (2021) 114613, https://doi.org/10.1016/j.molliq.2020.114613.

[29] Y. Absalan, M. Gholizadeh, H.J. Choi, Magnetized solvents: characteristics and various applications, J. Mol. Liq. 335 (2021) 116167, https://doi.org/10.1016/j.molliq.2021.116167.

[30] J. Liu, Y. Cao, Experimental study on the surface tension of magnetized water, Int. Commun. Heat Mass Tran. 121 (2021) 105091, https://doi.org/10.1016/j.icheatmasstransfer.2020.105091.

[31] A. Hashemizadeh, M.J. Ameri, B. Aminshahidy, M. Gholizadeh, Influence and application of an external variable magnetic field on the aqueous HCL solution behavior: experimental study and modelling using the taguchi method, Appl. Chem. Eng. 29 (2018) 215–224, https://doi.org/10.14478/ace.2017.1119.

[32] S. Sarhadi, M. Gholizadeh, T. Moghadasian, S. Golmohammadzadeh, Moisturizing effects of solid lipid nanoparticles (SLN) and nanostructured lipid carriers (NLC) using deionized and magnetized water by in vivo and in vitro methods, Iran. J. Basic Med. Sci. 23 (2020) 337–343, https://doi.org/10.22038/IJBMS.2020.39587.9397.

[33] A.A.M. Al-Kuhla, The effect of magnetized water on growth and quality improvement of poultry, J. Glob. Innov. Agric. Sci. 11 (2023) 607–610, https://doi.org/10.22194/JGIAS/23.1097.

[34] K. El-Sabrout, M. Hanafy, Effect of magnetized water on productive traits of laying chickens, Prof. Anim. Sci. 33 (2017) 739–742, https://doi.org/10.15232/pas.2017-01656.

[35] S. Lin, Q. Wang, K. Wei, Y. Sun, F. Shao, Q. Lei, M. Deng, Enhancing pakchoi (Brassica chinensis L.) agriculture with magnetized-ionized brackish water and organic fertilizers: a sustainable approach to soil quality and crop yield optimization, J. Clean. Prod. 450 (2024) 141935, https://doi.org/10.1016/j.jclepro.2024.141935.

[36] J. Dobránszki, From mystery to reality: magnetized water to tackle the challenges of climate change and for cleaner agricultural production, J. Clean. Prod. 425 (2023), https://doi.org/10.1016/j.jclepro.2023.139077.

[37] D. Rani, K. Kobtrakul, W. De-Eknamkul, S. Vimolmangkang, Magnetized water: a way to enhance isoflavonoids in cultured Pueraria candollei var. mirifica cells, Ind. Crops Prod. 180 (2022) 114779, https://doi.org/10.1016/j.indcrop.2022.114779.

[38] M.A.H. Al-Akhras, N.A. Al-Quraan, Z.A. Abu-Aloush, M.S. Mousa, T. AlZoubi, G. N. Makhadmeh, O. Donmez, K. Al jarrah, Impact of magnetized water on seed germination and seedling growth of wheat and barley, Results Eng. 22 (2024) 101991, https://doi.org/10.1016/j.rineng.2024.101991.

[39] S. Ghorbani, S. Ghorbani, A. Elmi, V. Soleimani, I. Taji, M. Mohammadi-Khatami, M. Tavakkolizadeh, J. de Brito, Simultaneous effect of granite waste dust as partial replacement of cement and magnetized water on the properties of concrete exposed to NaCl and $H_2SO_4$ solutions, Constr. Build. Mater. 288 (2021) 123064, https://doi.org/10.1016/j.conbuildmat.2021.123064.

[40] G. Zhao, Z. Zhang, N. Ma, Y. Wang, S. Cheng, Preparation and characterization of cement mortar mixed with alternating field-magnetized water, Constr. Build. Mater. 416 (2024) 135204, https://doi.org/10.1016/j.conbuildmat.2024.135204.

[41] A. Hashemizadeh, M. Gholizadeh, A. Tabatabaeinejad, M. Hoopanah, The possibility of enhanced oil recovery by using magnetic water flooding, Petrol. Sci. Technol. 32 (2014) 1038–1042, https://doi.org/10.1080/10916466.2011.634875.

[42] C. Sronsri, K. U-yen, W. Sittipol, Quantitative analysis of calcium carbonate formation in magnetized water, Mater. Chem. Phys. 245 (2020), https://doi.org/10.1016/j.matchemphys.2020.122735.

[43] Y. Absalan, M. Gholizadeh, V.V. Kopylov, L.A. Butusov, V. Bagherzadeh, S.H. H. Sajed, O.V. Kovalchukova, Investigation an environmentally friendly method under magnetic field as a green solvent for the synthesis of brookite phase nanoparticles at room temperature, J. Mater. Sci. Mater. Electron. 32 (2021) 12535–12546, https://doi.org/10.1007/s10854-021-05889-4.

[44] M. Bakherad, R. Doosti, A. Keivanloo, M. Gholizadeh, A.H. Amin, A. New, Simple, catalyst-free method for the synthesis of pyrazolopyranopyrimidines in magnetized

water, Lett. Org. Chem. 14 (2017) 510–516, https://doi.org/10.2174/1570178614666170511170329.
[45] M. Gholizadeh, Process of Chemical Reaction in Magnetized Solvents, 2019 (US10507450B2).
[46] Z. Yu, J. Deschamps, L. Hamon, P. Karikkethu Prabhakaran, P. Pré, Modeling hydrogen diffusion in hybrid activated carbon-MIL-101(Cr) considering temperature variations and surface loading changes, Microporous Mesoporous Mater. 248 (2017) 72–83, https://doi.org/10.1016/j.micromeso.2017.03.059.
[47] U.A. Adamu, N.H.H. Abu Bakar, Z.U. Zango, N.S. Sambudi, A. Iqbal, M.H. Hussin, T.S. Hamidon, Low-temperature synthesis and characterization of porous chromium terephthalate MIL-101(Cr) and its photocatalytic degradation of phenanthrene, Kor. J. Chem. Eng. 40 (2023) 2239–2252, https://doi.org/10.1007/s11814-023-1408-0.
[48] R. Bagheri, M. Ghaedi, A. Asfaram, E. Alipanahpour Dil, H. Javadian, RSM-CCD design of malachite green adsorption onto activated carbon with multimodal pore size distribution prepared from Amygdalus scoparia: kinetic and isotherm studies, Polyhedron 171 (2019) 464–472, https://doi.org/10.1016/j.poly.2019.07.037.
[49] H. Hajjaoui, A. Soufi, H. Khiar, M. Abdennouri, M. Achak, N. Barka, Preparation of sodium zinc phosphate/polyaniline nanocomposite for Cr(VI) and eriochrome black T adsorption from water, Mater. Today Commun. 36 (2023) 106755, https://doi.org/10.1016/j.mtcomm.2023.106755.
[50] R. Cai, H. Yang, J. He, W. Zhu, The effects of magnetic fields on water molecular hydrogen bonds, J. Mol. Struct. 938 (2009) 15–19, https://doi.org/10.1016/j.molstruc.2009.08.037.
[51] H.X. Hu, C. Deng, Effect of magnetized water on the stability and consolidation compressive strength of cement grout, Materials (Basel) 14 (2021) 1–18, https://doi.org/10.3390/ma14020275.
[52] N. Emamdadi, M. Gholizadeh, M.R. Housaindokht, The effect of magnetized water on the oxidation reaction of phenol derivatives and aromatic amines by horseradish peroxidase enzyme, Biotechnol. Prog. 36 (2020) 1–11, https://doi.org/10.1002/btpr.3035.
[53] A. Mohammadnezhad, S. Azizi, H. Sousanabadi Farahani, J. Tashan, A. Habibnejad Korayem, Understanding the magnetizing process of water and its effects on cementitious materials: a critical review, Constr. Build. Mater. 356 (2022) 129076, https://doi.org/10.1016/j.conbuildmat.2022.129076.
[54] A.A. Rico-Barragán, J. Raziel Álvarez, E. Hernández-Fernández, J. Rodríguez-Hernández, M.A. Garza-Navarro, N.E. Dávila-Guzmán, Green synthesis of metal-organic framework MIL-101(Cr) – an assessment by quantitative green chemistry metrics, Polyhedron 225 (2022), https://doi.org/10.1016/j.poly.2022.116052.
[55] X. Zhang, F. Wei, T. Bao, S. Wang, Target adsorption of indomethacin sodium from aqueous solutions using mixed-ligand MIL-101(Cr), J. Solid State Chem. 311 (2022), https://doi.org/10.1016/j.jssc.2022.123098.
[56] U.A. Adamu, N.H.H. Abu Bakar, A. Iqbal, N.S. Sambudi, Z.U. Zango, The role of bio-inspired ZnO nanoparticles in the modification of MIL101(Cr) properties for visible light degradation of phenanthrene, Catal. Commun. 187 (2024) 106905, https://doi.org/10.1016/j.catcom.2024.106905.
[57] M.S. Alivand, N.H.M.H. Tehrani, M. Askarieh, E. Ghasemy, M.D. Esrafili, R. Ahmadi, H. Anisi, O. Tavakoli, A. Rashidi, Defect engineering-induced porosity in graphene quantum dots embedded metal-organic frameworks for enhanced benzene and toluene adsorption, J. Hazard. Mater. 416 (2021), https://doi.org/10.1016/j.jhazmat.2021.125973.
[58] E. Esmaeilnezhad, H.J. Choi, M. Schaffie, M. Gholizadeh, M. Ranjbar, Characteristics and applications of magnetized water as a green technology, J. Clean. Prod. 161 (2017) 908–921, https://doi.org/10.1016/j.jclepro.2017.05.166.
[59] M.Y. Zorainy, M. Gar Alalm, S. Kaliaguine, D.C. Boffito, Revisiting the MIL-101 metal-organic framework: design, synthesis, modifications, advances, and recent applications, J. Mater. Chem. A 9 (2021) 22159–22217, https://doi.org/10.1039/d1ta06238g.
[60] N.C. Burtch, H. Jasuja, K.S. Walton, Water stability and adsorption in metal-organic frameworks, Chem. Rev. 114 (2014) 10575–10612, https://doi.org/10.1021/cr5002589.
[61] P.K. Roy, E. Bormashenko, M. Frenkel, I. Legchenkova, S. Shoval, Magnetic field induced motion of water droplets and bubbles on the lubricant coated surface, Colloids Surfaces A Physicochem. Eng. Asp. 597 (2020) 124773, https://doi.org/10.1016/j.colsurfa.2020.124773.
[62] P. Premkaisorn, W. Wasupongpun, Magnetic field effect on properties of water, RMUTP Res. J. 14 (2020) 1–17.
[63] Y. Fujimura, M. Iino, Magnetic field increases the surface tension of water, J. Phys. Conf. Ser. 156 (2009), https://doi.org/10.1088/1742-6596/156/1/012028.
[64] C. Deng, L. Li, H. Hu, Z. Xu, Y. Zhou, Q. Yin, J. Chen, Effect of magnetized water on the fundamental grouting properties of cement grout under varying magnetization conditions, Sci. Rep. 15 (2025) 1–26, https://doi.org/10.1038/s41598-024-84928-6.
[65] J. Tripathi, M. Gupta, A. Yadav, K. Waghmode, P. More, Metal–organic framework MIL-101(Cr): an efficient catalyst for the synthesis of biphenyls and biphenyl diols, Res. Chem. Intermed. 50 (2024) 1645–1660, https://doi.org/10.1007/s11164-024-05240-6.
[66] N. Ko, P.G. Choi, J. Hong, M. Yeo, S. Sung, K.E. Cordova, H.J. Park, J.K. Yang, J. Kim, Tailoring the water adsorption properties of MIL-101 metal-organic frameworks by partial functionalization, J. Mater. Chem. A 3 (2015) 2057–2064, https://doi.org/10.1039/c4ta04907a.
[67] M. Mehralian, Z. Goodarzvand Chegini, M. Khashij, Activated carbon prepared from pistachio waste for dye adsorption: experimental and CCD-based design, Pigment Resin Technol. 49 (2020) 136–144, https://doi.org/10.1108/PRT-06-2019-0052.
[68] S.M. Pourmoheb Hosseini, N. Chaibakhsh, Efficient dye removal using $Fe_3O_4$.$MnO_2$.$MoS_2$ nanocomposite in optimized photocatalytic ozonation process, Ozone Sci. Eng. 45 (2023) 346–360, https://doi.org/10.1080/01919512.2022.2109590.
[69] L.K. Njaramba, M. Kim, Y. Yea, Y. Yoon, C.M. Park, Efficient adsorption of naproxen and ibuprofen by gelatin/zirconium-based metal–organic framework/sepiolite aerogels via synergistic mechanisms, Chem. Eng. J. 452 (2023), https://doi.org/10.1016/j.cej.2022.139426.
[70] H.E.L. Madsen, Influence of magnetic field on the precipitation of some inorganic salts, J. Cryst. Growth 152 (1995) 94–100, https://doi.org/10.1016/0022-0248(95)00103-4.
[71] X. Jia, S. Li, Y. Wang, T. Wang, X. Hou, Adsorption behavior and mechanism of sulfonamide antibiotics in aqueous solution on a novel MIL-101(Cr)@GO composite, J. Chem. Eng. Data 64 (2019) 1265–1274, https://doi.org/10.1021/acs.jced.8b01152.
[72] T. Wu, N. Prasetya, K. Li, Re-generable and re-synthesisable micro-structured MIL-53 Rachig Rings for ibuprofen removal, J. Environ. Chem. Eng. 10 (2022) 107432, https://doi.org/10.1016/j.jece.2022.107432.
[73] S. Sharifian, F. Farshchi Tabrizi, A. Sardarian, Efficient adsorptive removal of diclofenac sodium by acidified MIL101(Cr): optimizing the content of phosphotungstic acid, flow loop thin film slurry flat plate reactor, J. Porous Mater. 30 (2023) 975–988, https://doi.org/10.1007/s10934-022-01388-x.
[74] J. Jin, Z. Yang, W. Xiong, Y. Zhou, R. Xu, Y. Zhang, J. Cao, X. Li, C. Zhou, Cu and Co nanoparticles co-doped MIL-101 as a novel adsorbent for efficient removal of tetracycline from aqueous solutions, Sci. Total Environ. 650 (2019) 408–418, https://doi.org/10.1016/j.scitotenv.2018.08.434.
[75] B.M. Thamer, F.A. Al-aizari, H.S. Abdo, M.H. El-Newehy, Facile green fabrication of MIL-101(Cr)/PVA nanofiber composite as effective, stable, and reusable adsorbent for cationic dye removal, Polym. Eng. Sci. (2024) 1–17, https://doi.org/10.1002/pen.26922.
[76] L. Liang, F. Xi, J. Zhao, G. Imanova, S. Komarneni, J. Ma, Synergistic effect of MIL-101(Cr) and nanoscale zero-valent iron (nZVI) for efficient removal of U(VI) and assessment of this composite to inactivate Escherichia coli, Sep. Purif. Technol. 360 (2025), https://doi.org/10.1016/j.seppur.2024.131053.
[77] M.L. Chen, S.Y. Zhou, Z. Xu, L. Ding, Y.H. Cheng, Metal-organic frameworks of MIL-100(Fe, Cr) and MIL-101(Cr) for aromatic amines adsorption from aqueous solutions, Met. Fram. MIL-100(Fe, Cr) MIL-101(Cr) Aromat. Amin. Adsorpt. from Aqueous Solut. 100 (2019) 1–13.
[78] Y. Dong, X. Tian, S. Huang, A.N. Alodhayb, M. Zahid, MIL-101(Cr) entrapped polyol-synthesized iron promoted platinum bimetallic nanoparticles system for synergistic selective hydrogenation of cinnamaldehyde, Int. J. Hydrogen Energy 86 (2024) 132–142, https://doi.org/10.1016/j.ijhydene.2024.08.122.